Supplement of Atmos. Chem. Phys., 26, 5249–5291, 2026
https://doi.org/10.5194/acp-26-5249-2026-supplement

Atmospheric Chemistry and Physics
Open Access
EGU

Supplement of

Evaluation of stratospheric transport in three generations of Chemistry-Climate Models

Marta Abalos et al.

Correspondence to: Marta Abalos (mabalosa@ucm.es)

This Supplementary Material presents additional figures. Most of them are analogous to those in the main document but showing the individual behavior for each model.

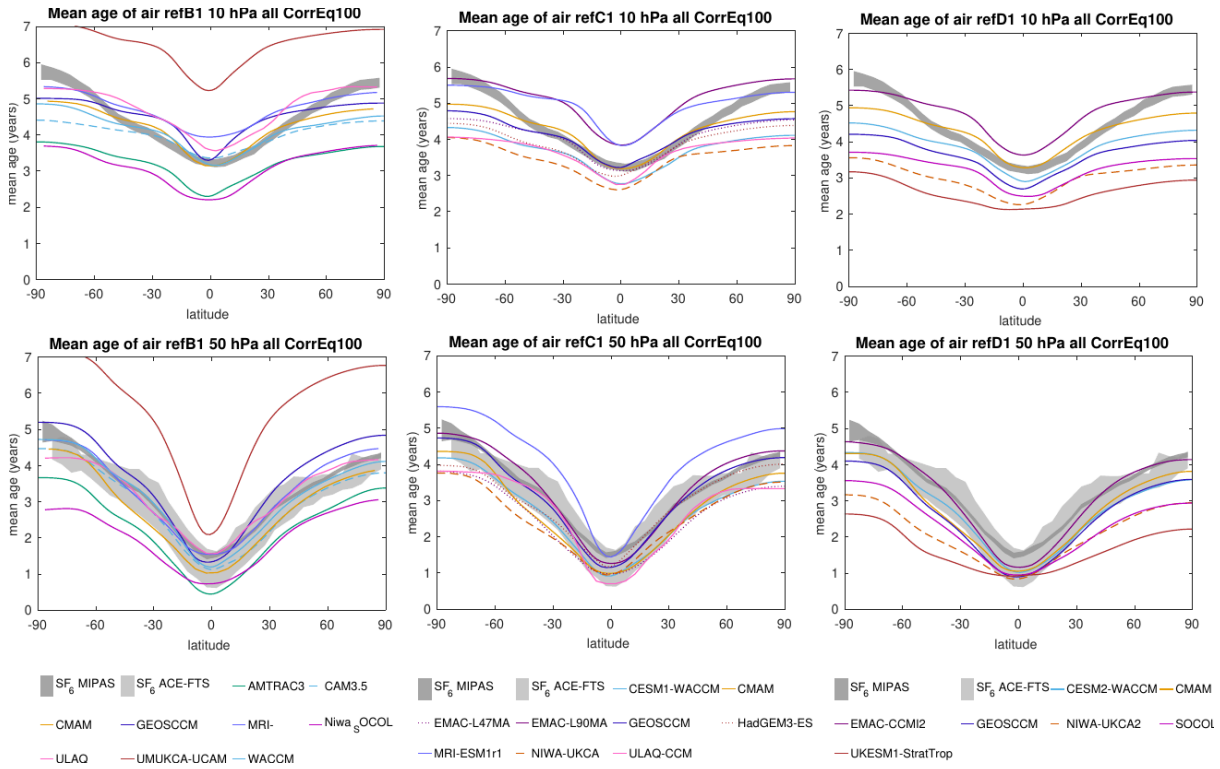

Figure S1. Latitudinal structure of mean age of air in individual models participating in the three intercomparison initiatives (lines) and observational estimates (shading). Mean age values in each dataset are relative to the mean age at the equator and 100 hPa. Levels: 10 hPa (top row) and 50 hPa (bottom row).Time period considered for averages: 1990-2010 (1980-2000 for refB1).

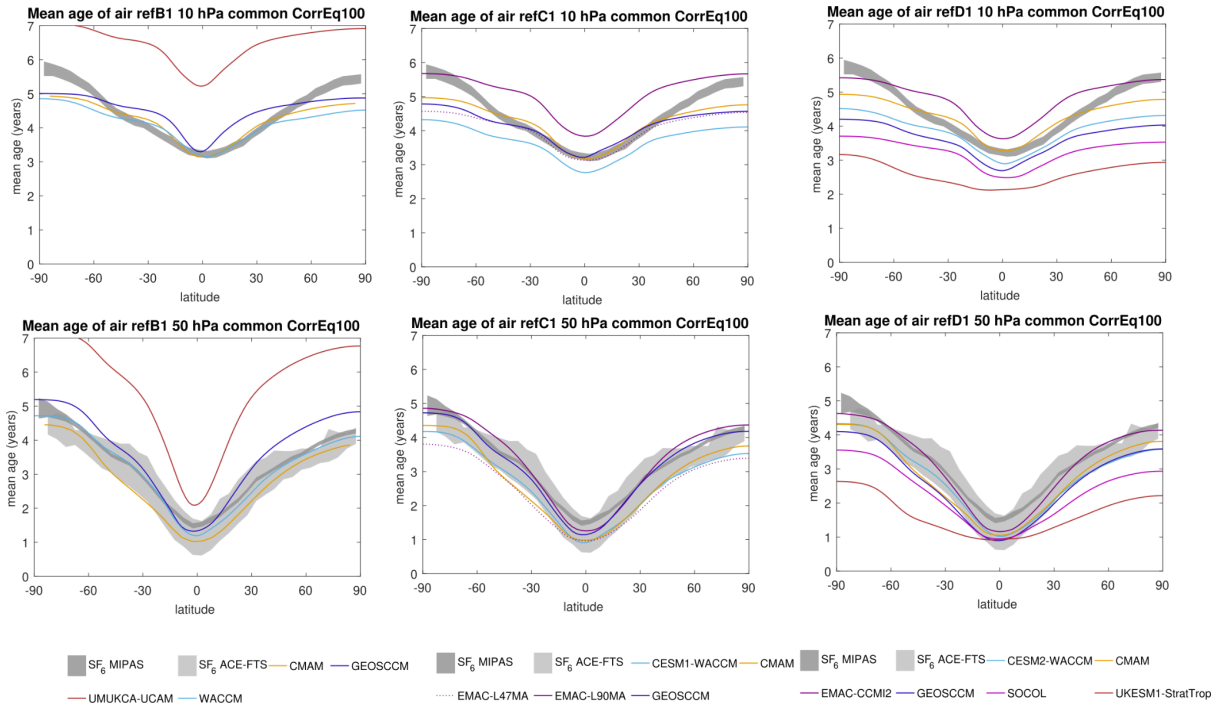

Figure S2. As Fig. S1 but for common models only, that is, models in the eight families identified in Tables 1-3 of the main manuscript.

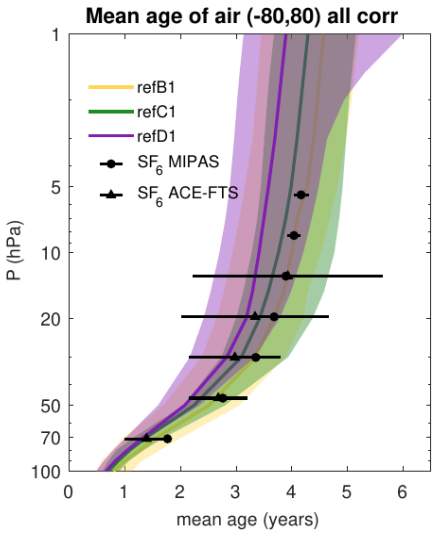

Figure S3. Vertical structure of quasi-global (80ºS-80ºN) mean age of air in the three generations of CCMs and in observational datasets.

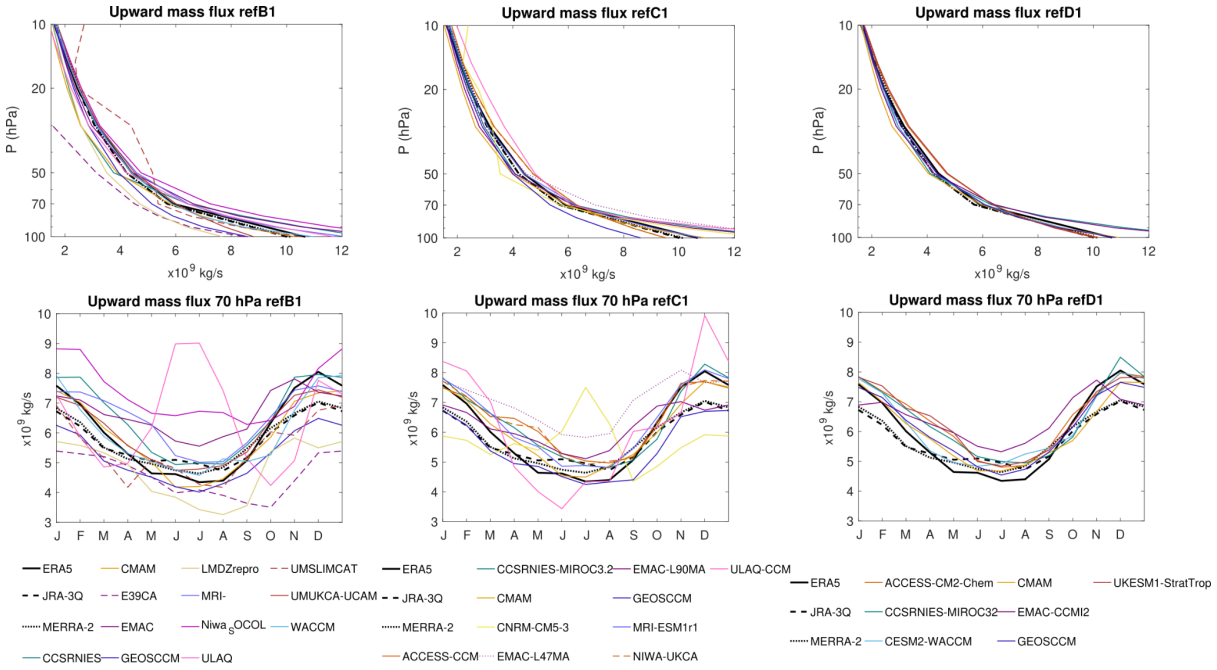

Figure S4. Annual mean vertical profile (top row) and seasonal cycle at 70 hPa (bottom row) of upward mass flux in individual models participating in the three intercomparison initiatives and three reanalyses. Average period: 1990-2010 (1990-2000 for refB1).

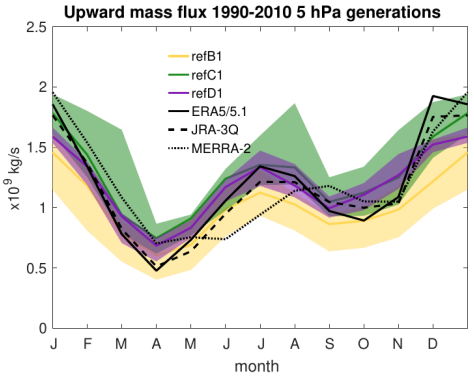

Figure S5. Annual cycle of net upward mass flux at 5 hPa.

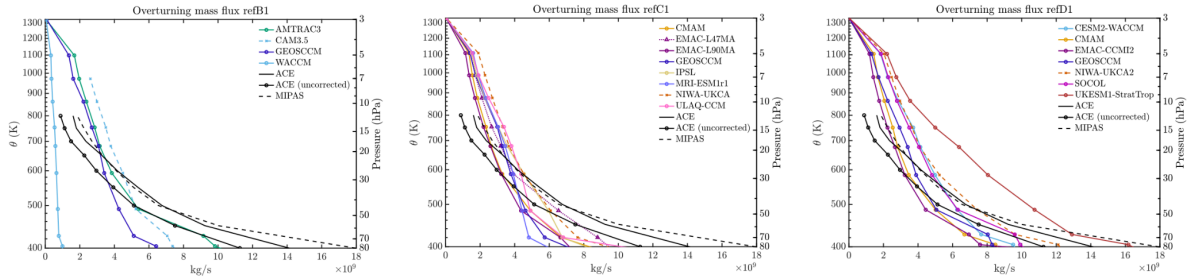

Figure S6. Overturning mass flux from mean age of air meridional gradient for all individual models participating in the three intercomparison initiatives.

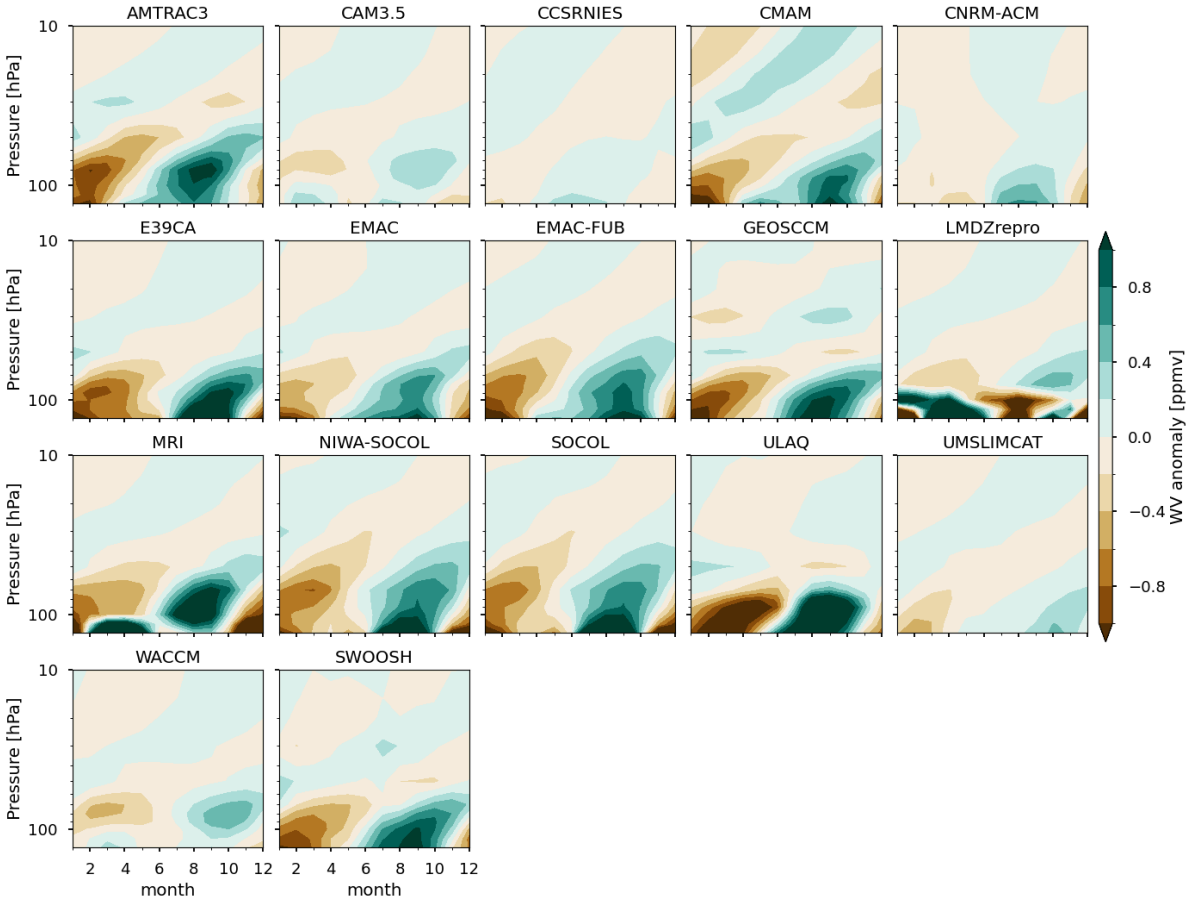

Figure S7. Plots show the water vapor tape recorder anomalies for each refB1 model and SWOOSH (lower- and right-most panel). The anomaly is defined as the departure from the annual climatological mean value at each level. The climatological base period for all datasets is 1992 - 2005.

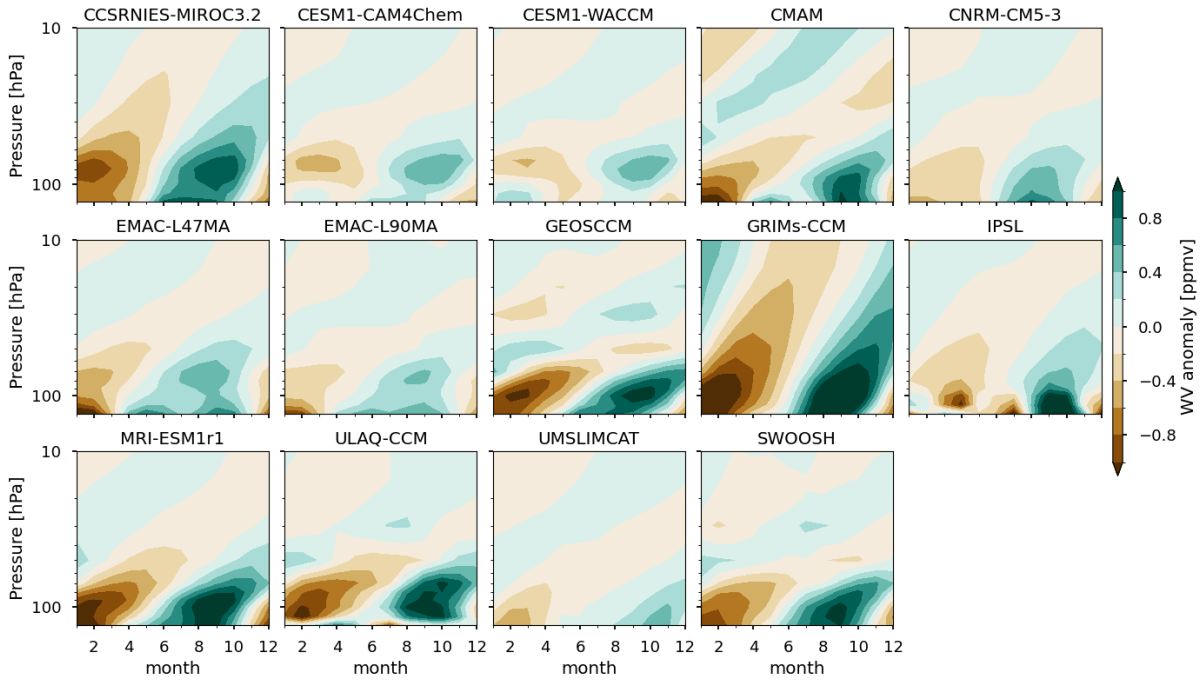

Fig. S8. As Fig. S7, but for refC1 using a 2005-2012 base period.

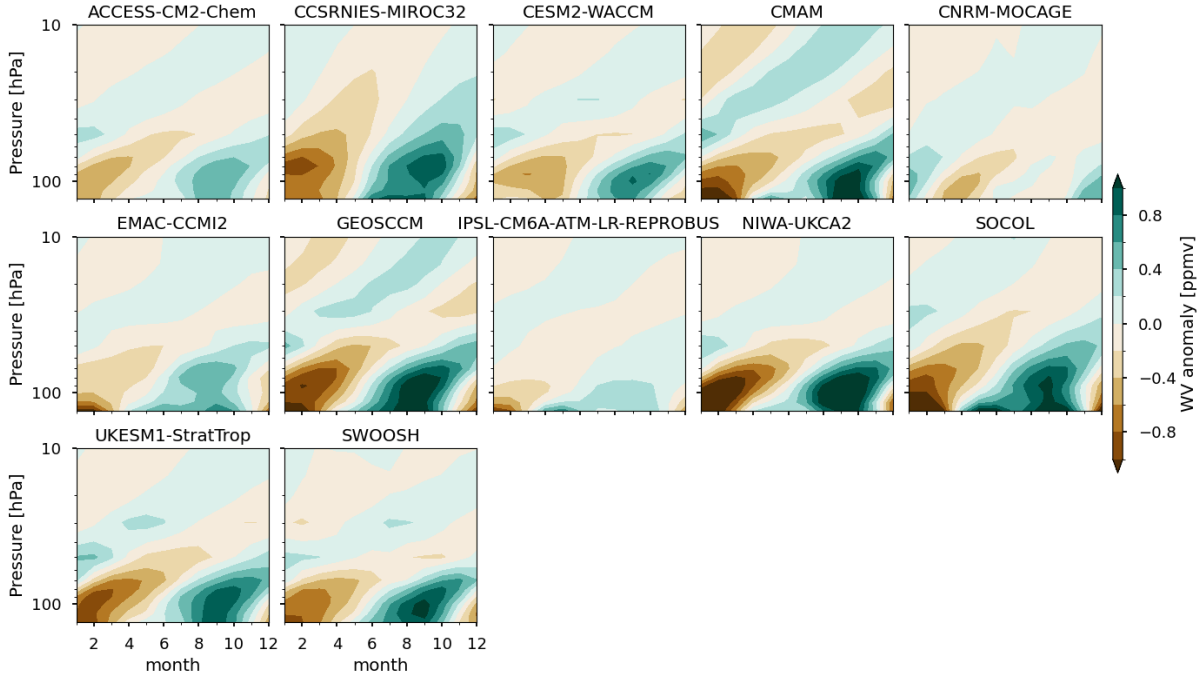

Figure S9. Same as Fig. S7, but for refD1 models using a 2005 - 2018 base period.

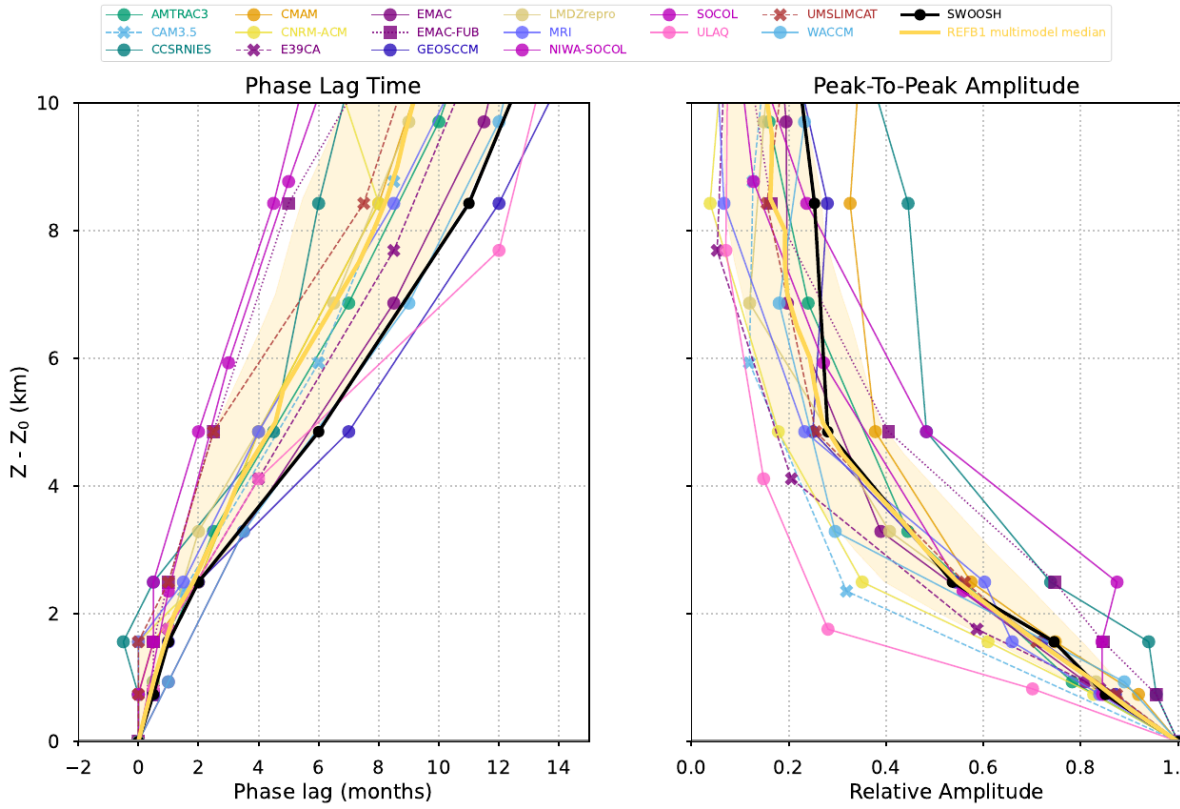
AMTRAC3
CAM3.5
CCSRNIES
CMAM
CNRM-ACM
E39CA
EMAC
EMAC-FUB
GEOSCCM
LMDZrepro
MRI
NIWA-SOCOL
SOCOL
ULAQ
UMSLIMCAT
WACCM
SWOOSH
REFB1 multimodel median
Phase Lag Time
Peak-To-Peak Amplitude
Z - Z0 (km)
Phase lag (months)
Relative Amplitude

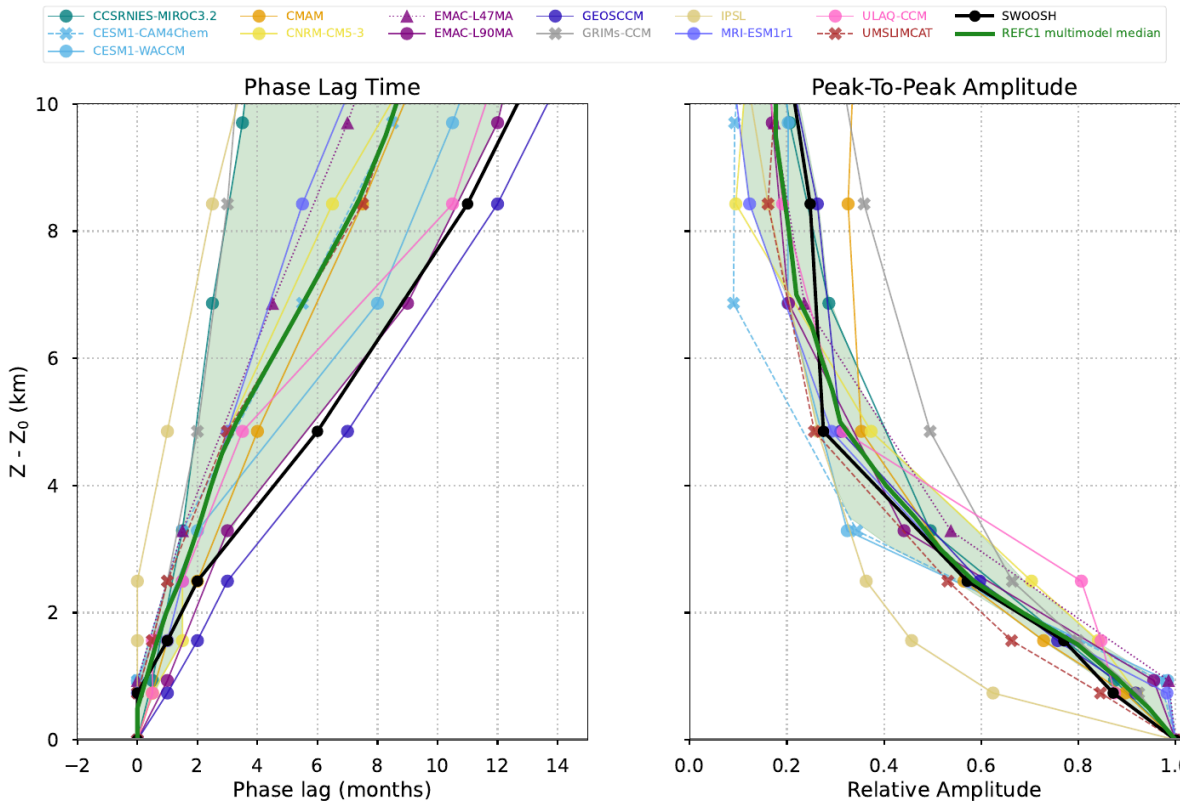
CCSRNIES-MIROC3.2
CESM1-CAM4Chem
CESM1-WACCM
CMAM
CNRM-CM5-3
EMAC-L47MA
EMAC-L90MA
GEOSCCM
GRIMs-CCM
IPSL
MRI-ESM1r1
ULAQ-CCM
UMSLIMCAT
SWOOSH
REFC1 multimodel median
Phase Lag Time
Peak-To-Peak Amplitude
Z - Z0 (km)
Phase lag (months)
Relative Amplitude

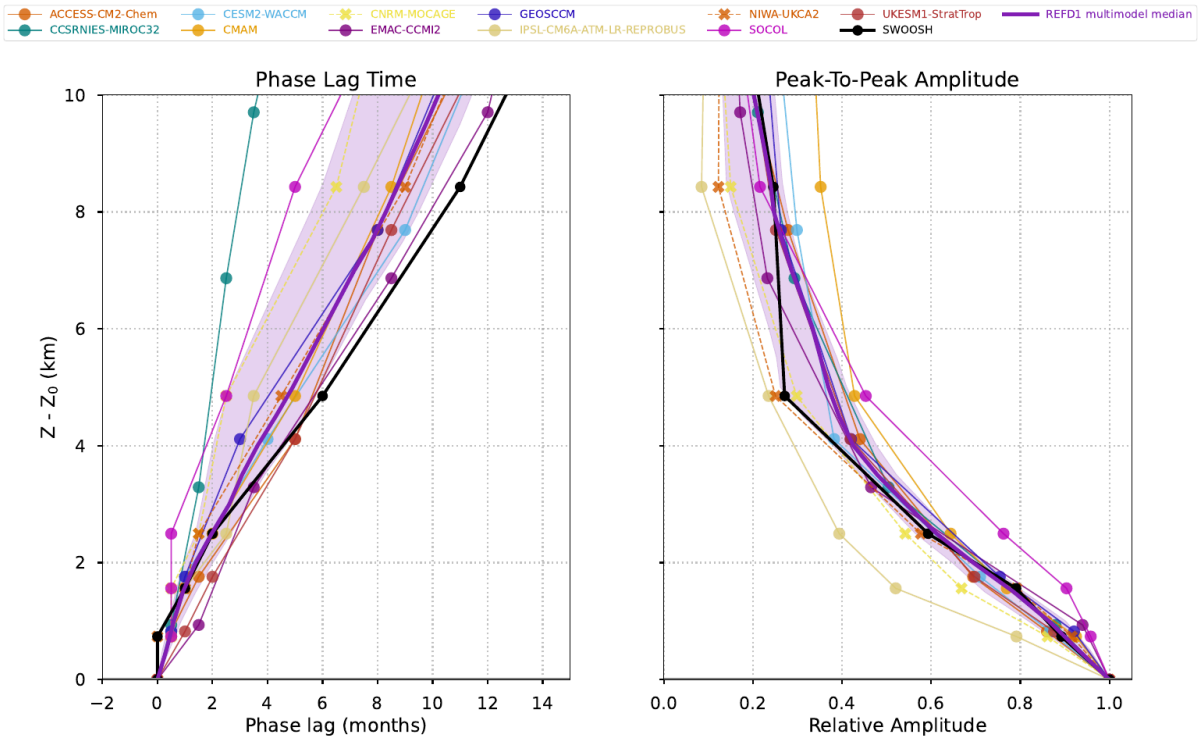

Figure S10. Phase and amplitude of tape recorder signal as a function of tropopause-relative altitude for individual models participating in the three intercomparison initiatives and the SWOOSH dataset.

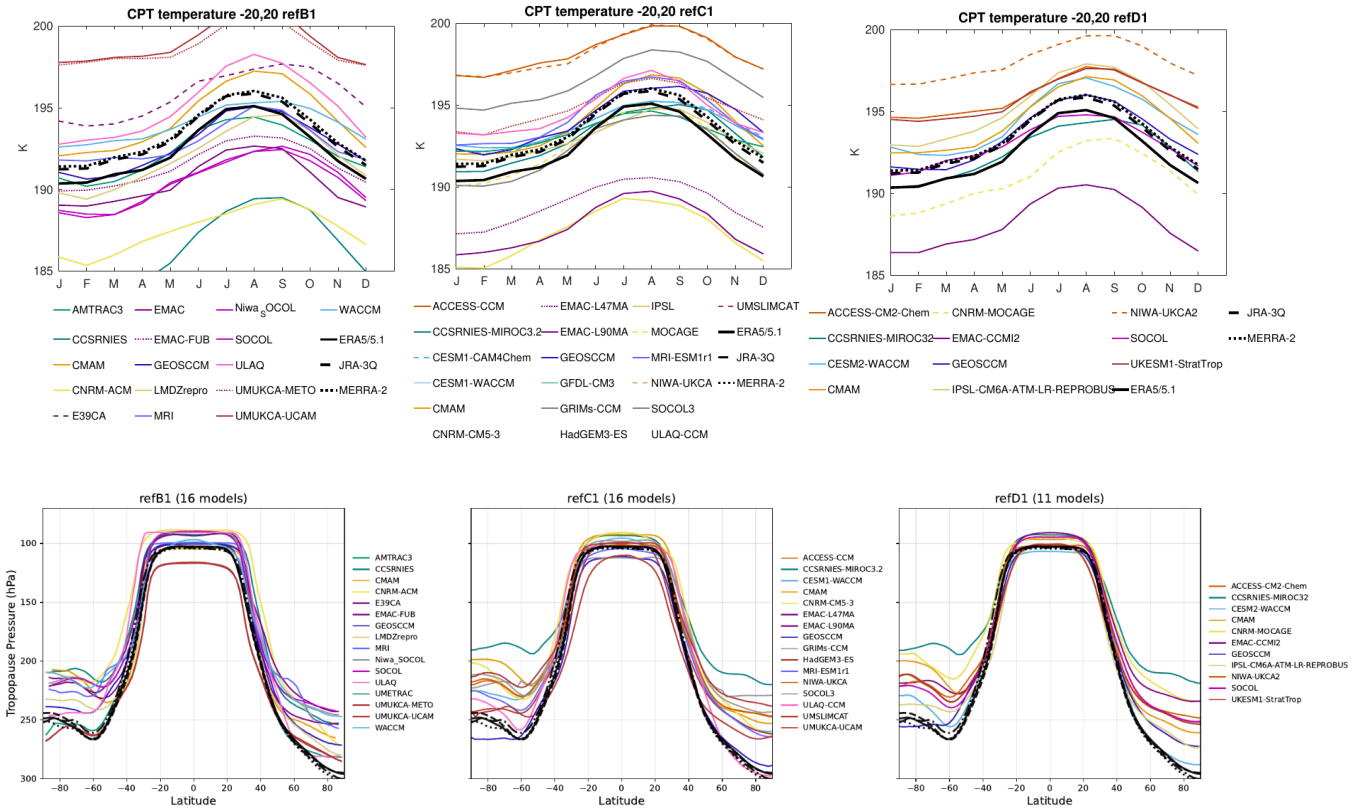

Figure S11. Cold-point tropopause temperature seasonal cycle (top panels) and annual mean lapse rate tropopause pressure as a function of latitude (bottom panels) for individual models participating in the three intercomparison initiatives and three reanalyses.

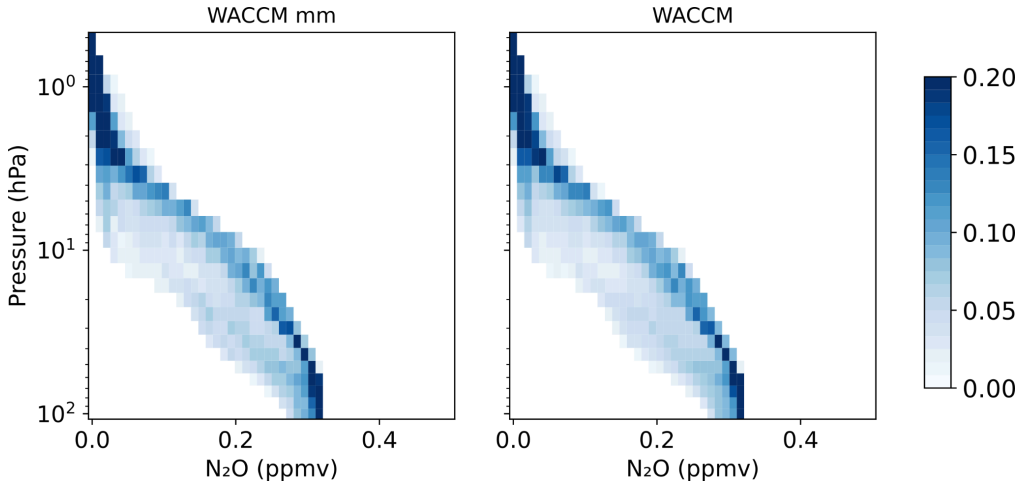

Figure S12. N2O PDF for CESM1-WACCM using daily mean (right panel) versus monthly mean (left) output.

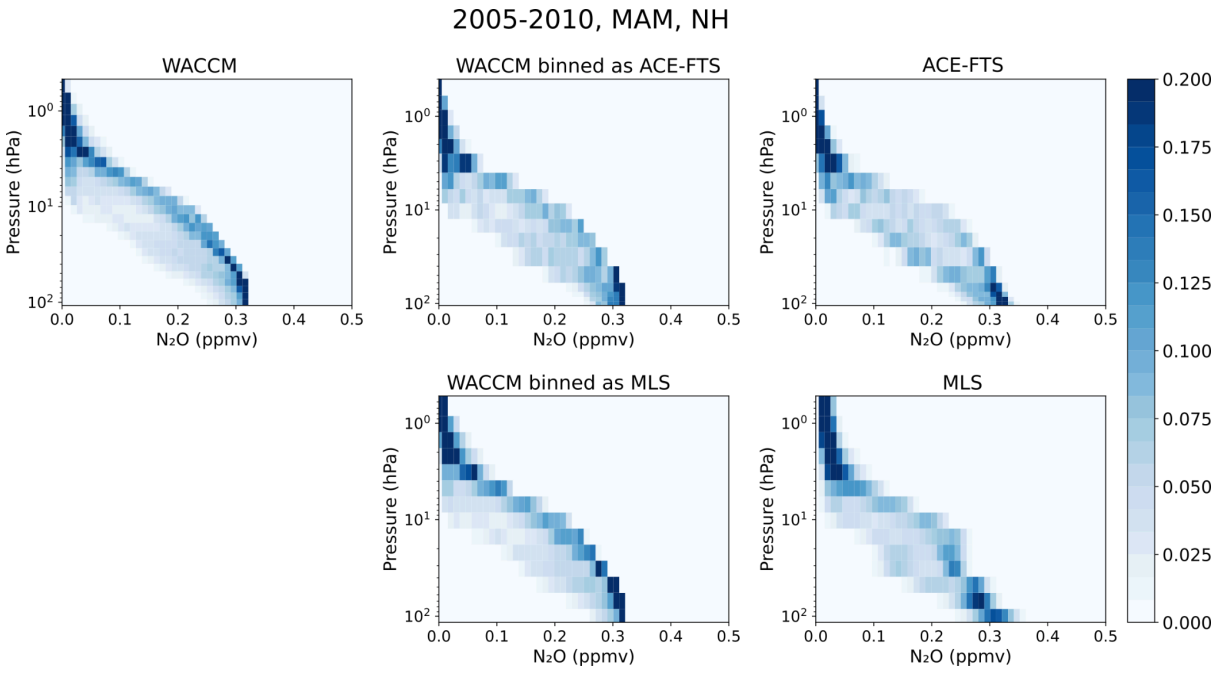

Figure S13. N2O PDF for CESM1-WACCM using daily mean output with all spatial points (left panel) versus subsampling the model with the satellite trajectory for ACE-FTS (middle top panel) and MLS (middle bottom panel). The results for each satellite are shown in the right panels for comparison.

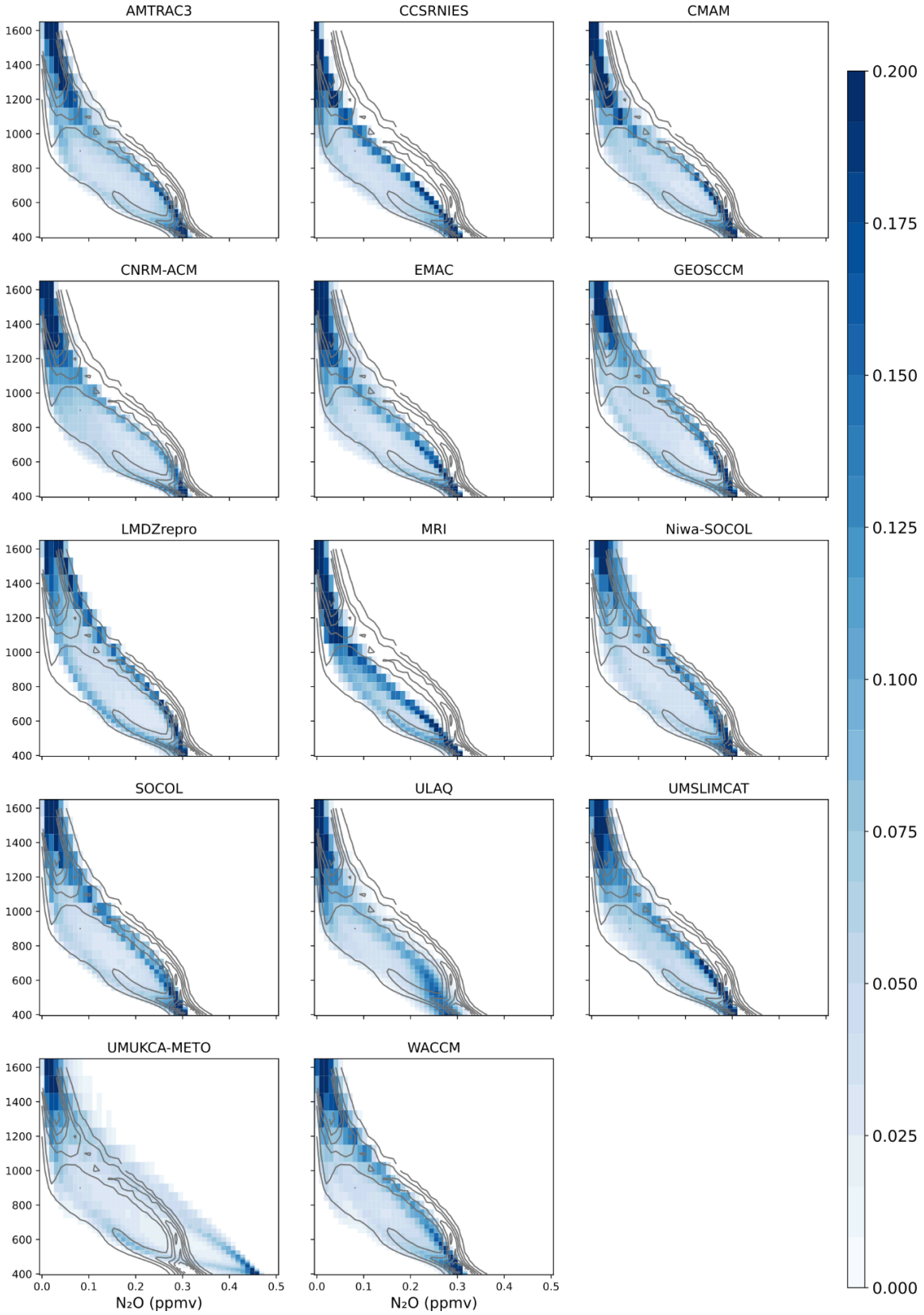

Figure S14. N2O PDF in NH spring (MAM) for individual refB1 models.

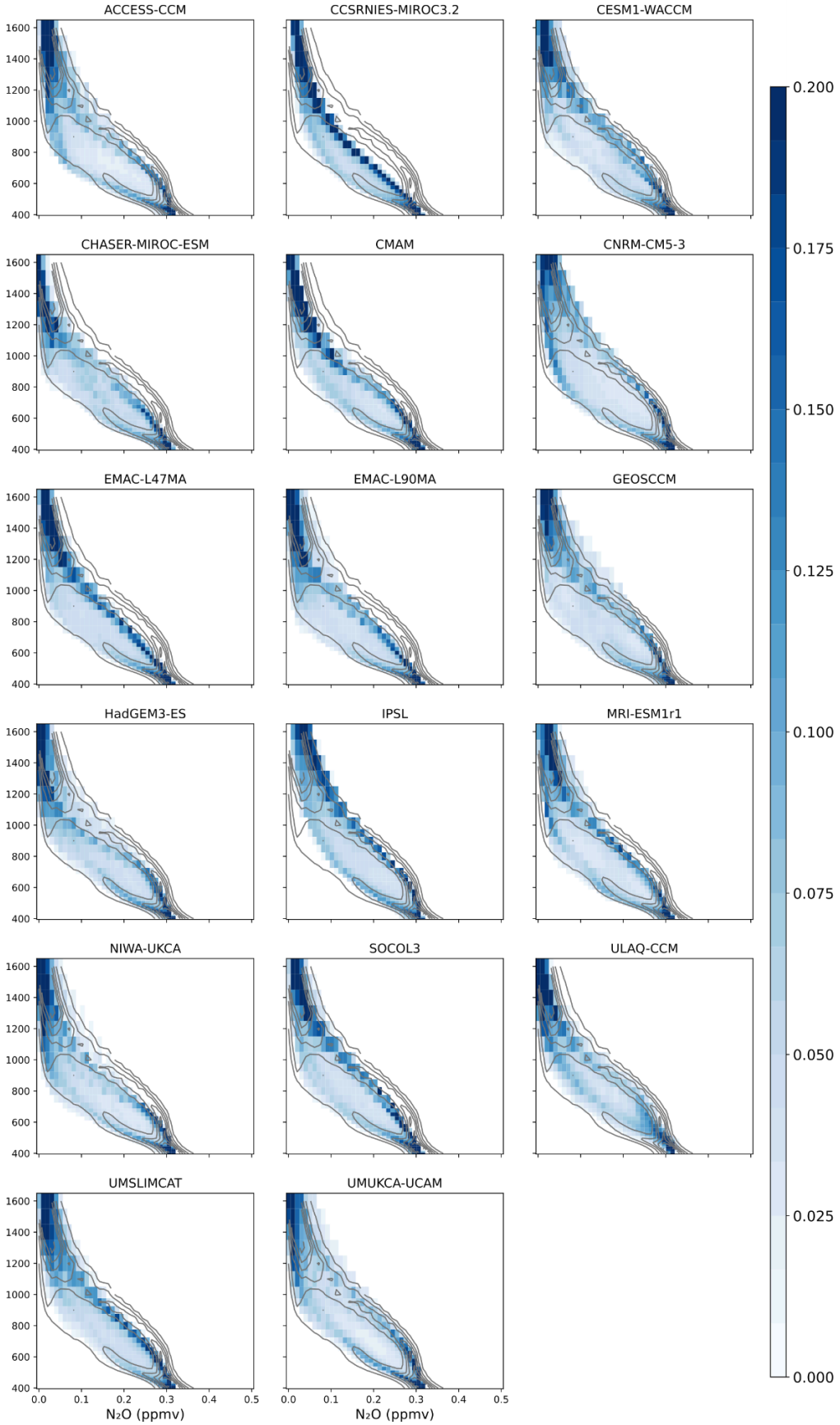

Figure S15. N2O PDF in NH spring (MAM) for individual refC1 models.

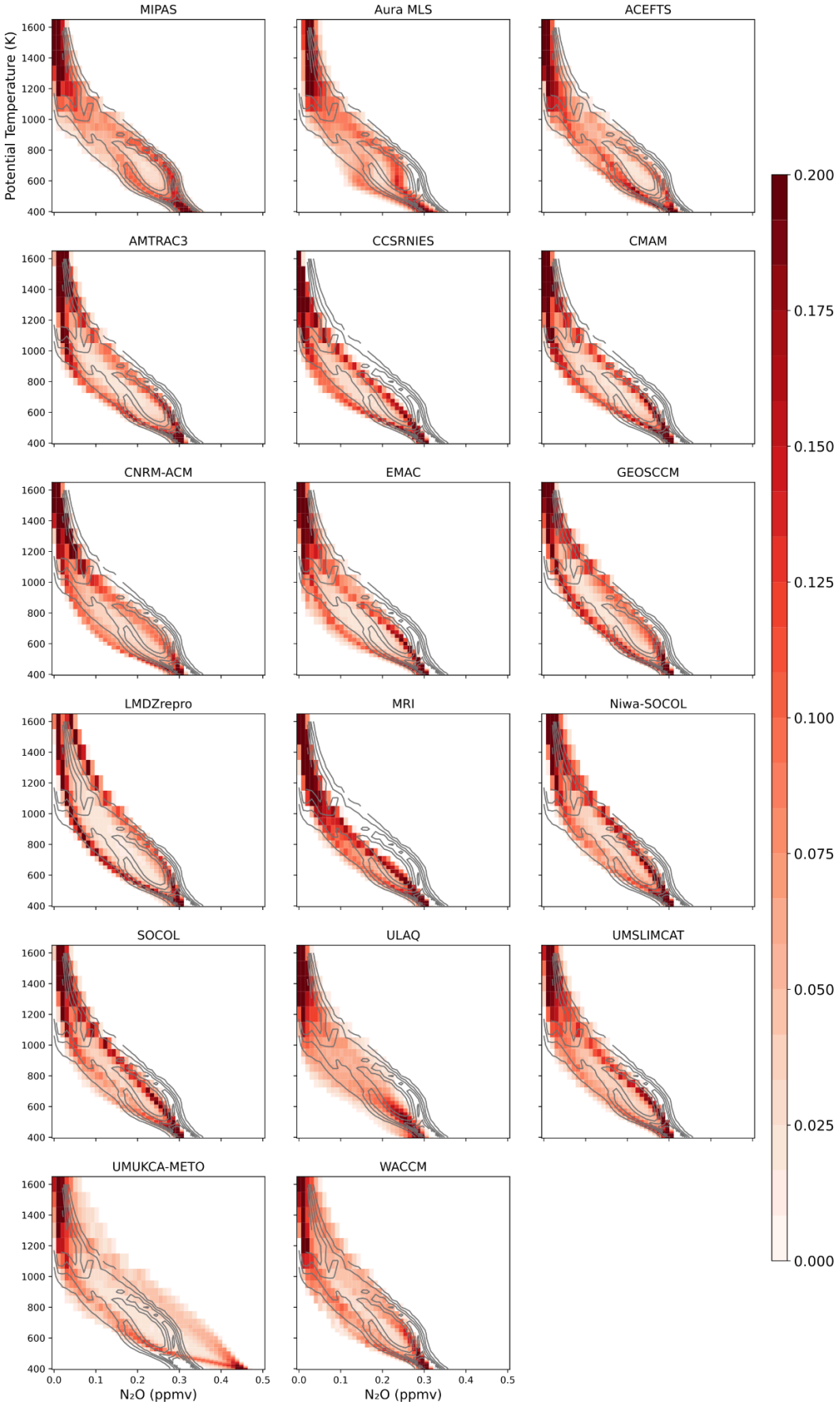

Figure S16. N2O PDF in SH spring (SON) for individual refB1 models.

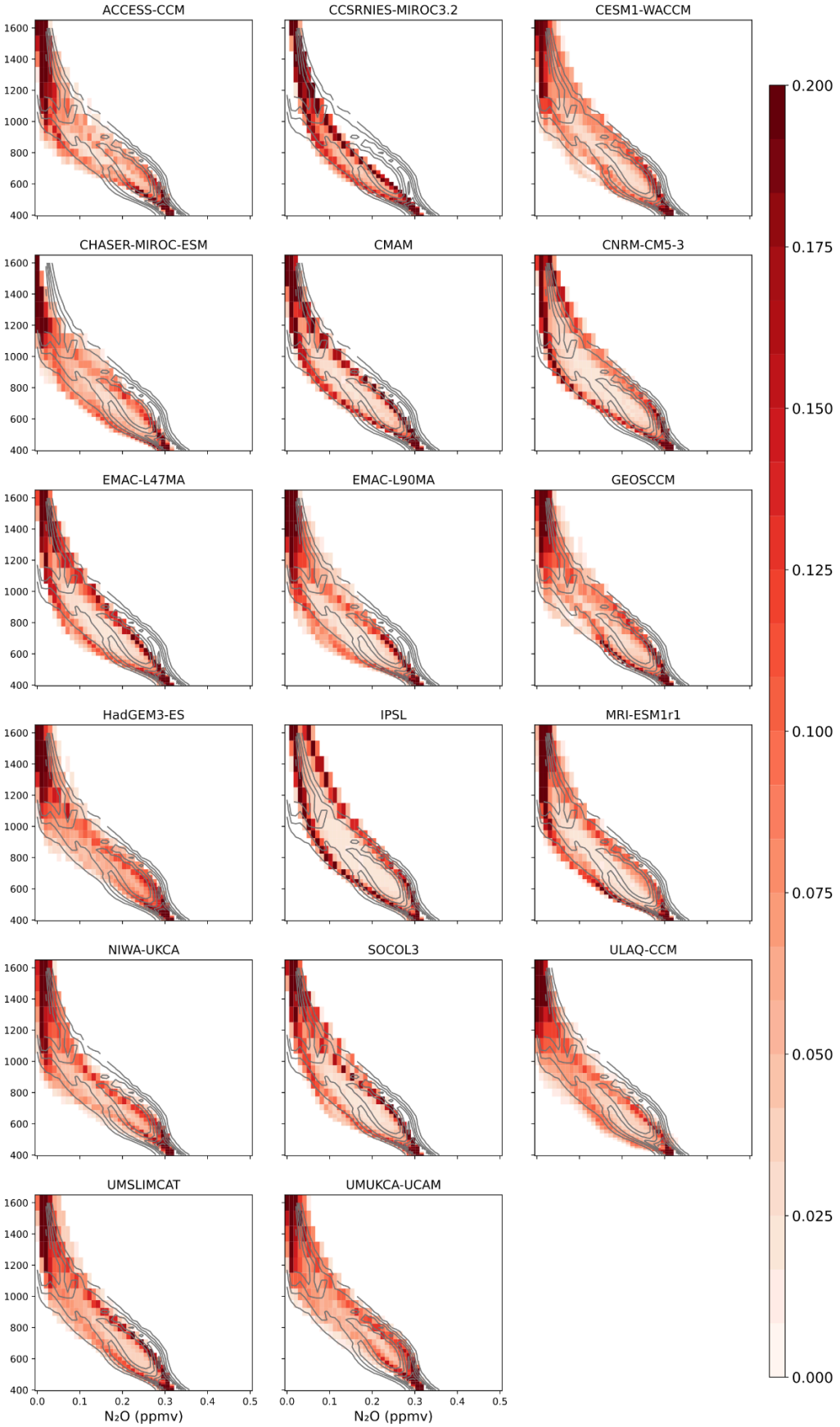

Figure S17. N2O PDF in SH spring (SON) for individual refC1 models.

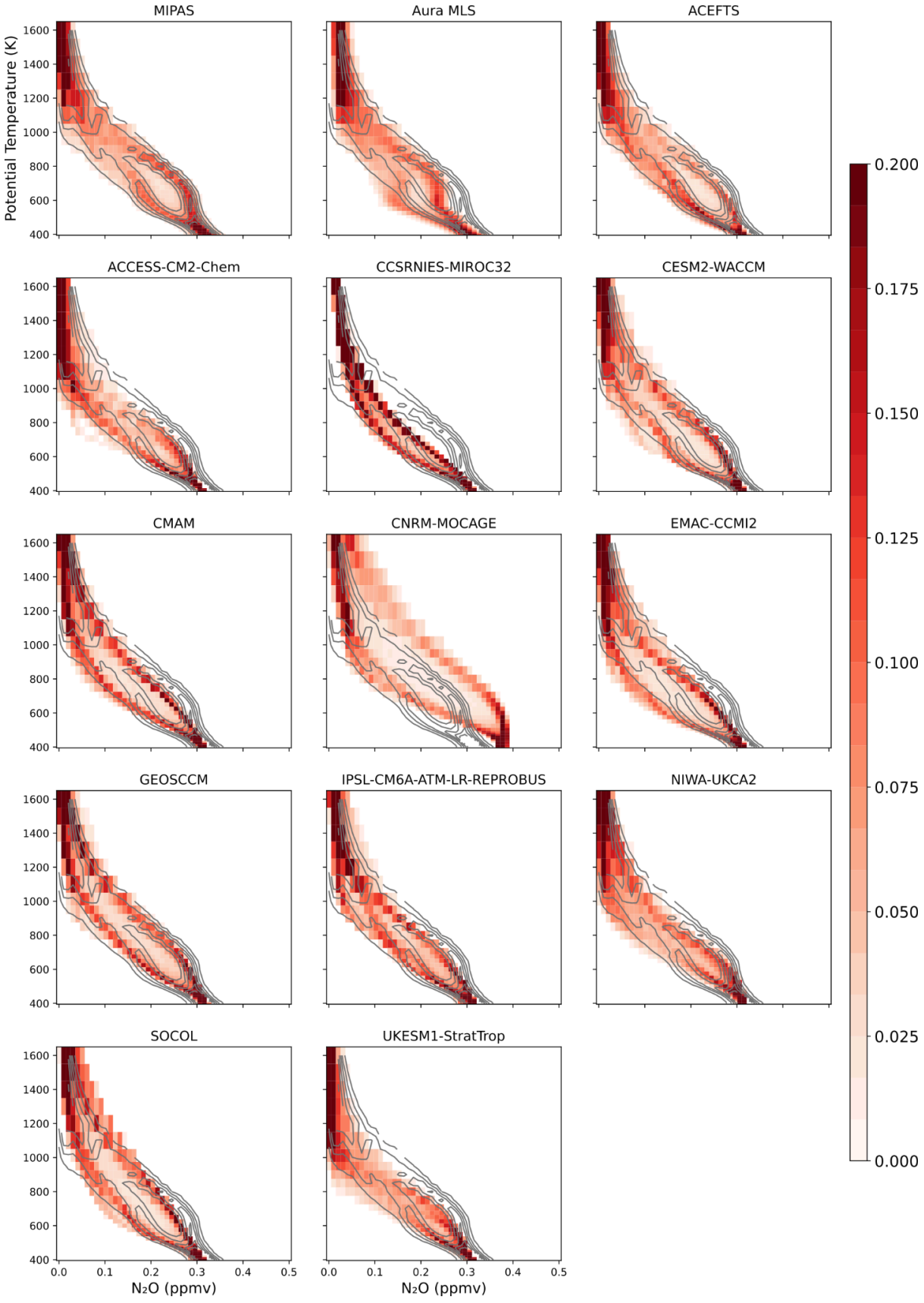

Figure S18. N2O PDF in SH spring (SON) for individual refD1 models.

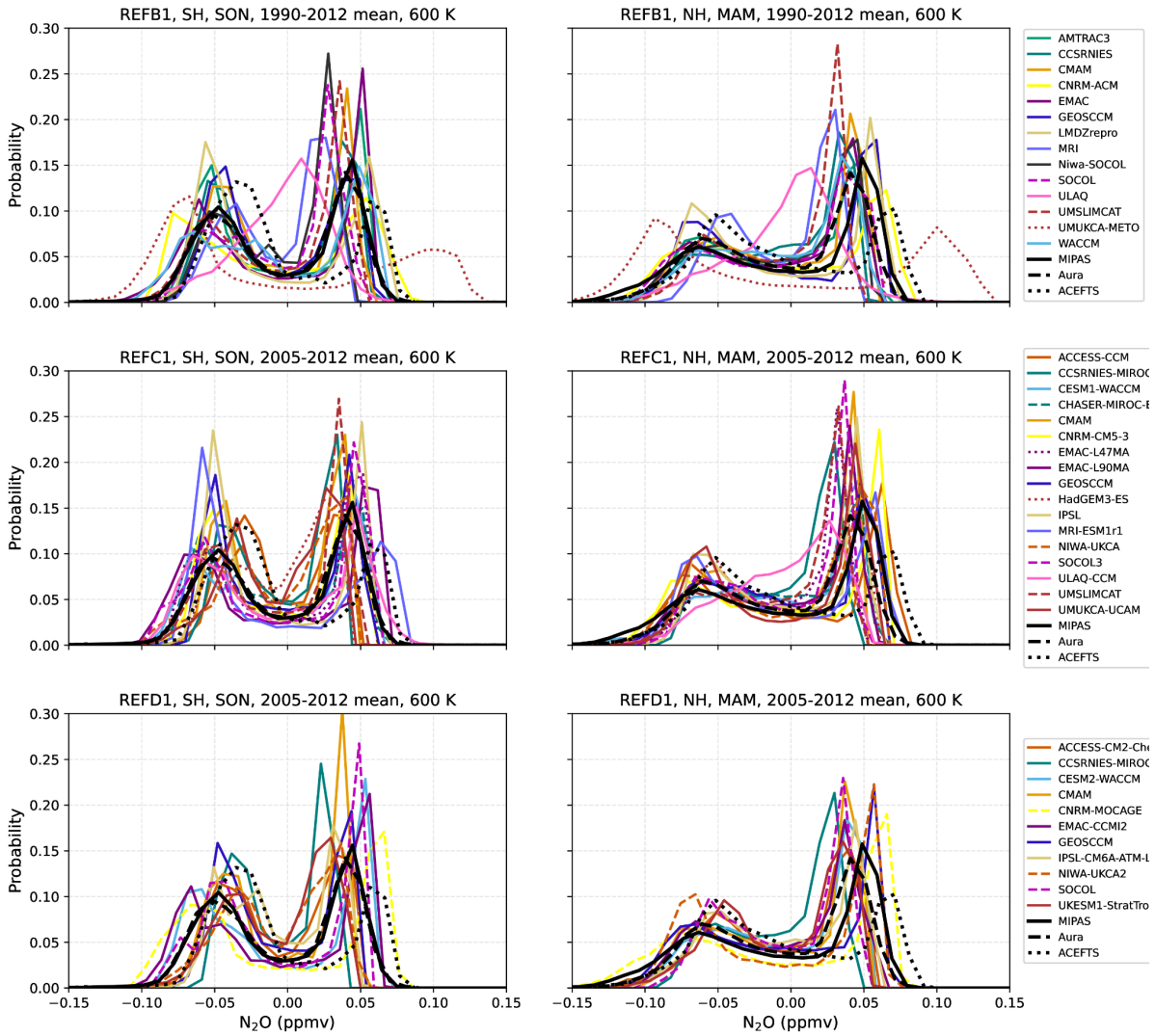

Figure S19. N2O PDF at 600 K for all individual models participating in the three intercomparison initiatives.

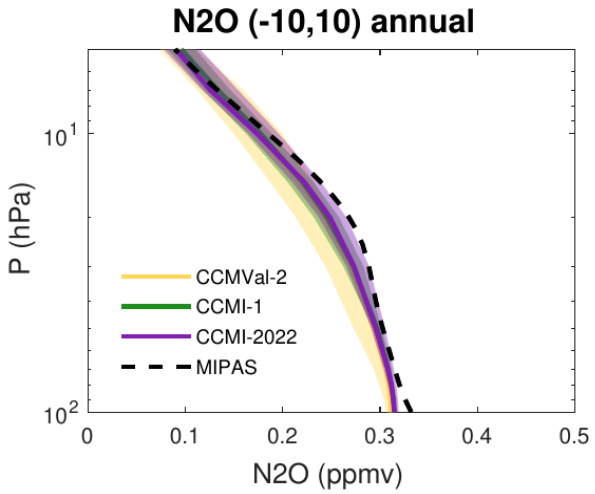

Figure S20. Vertical profile of the N2O tropical annual mean climatology for the three model generations and MIPAS data.

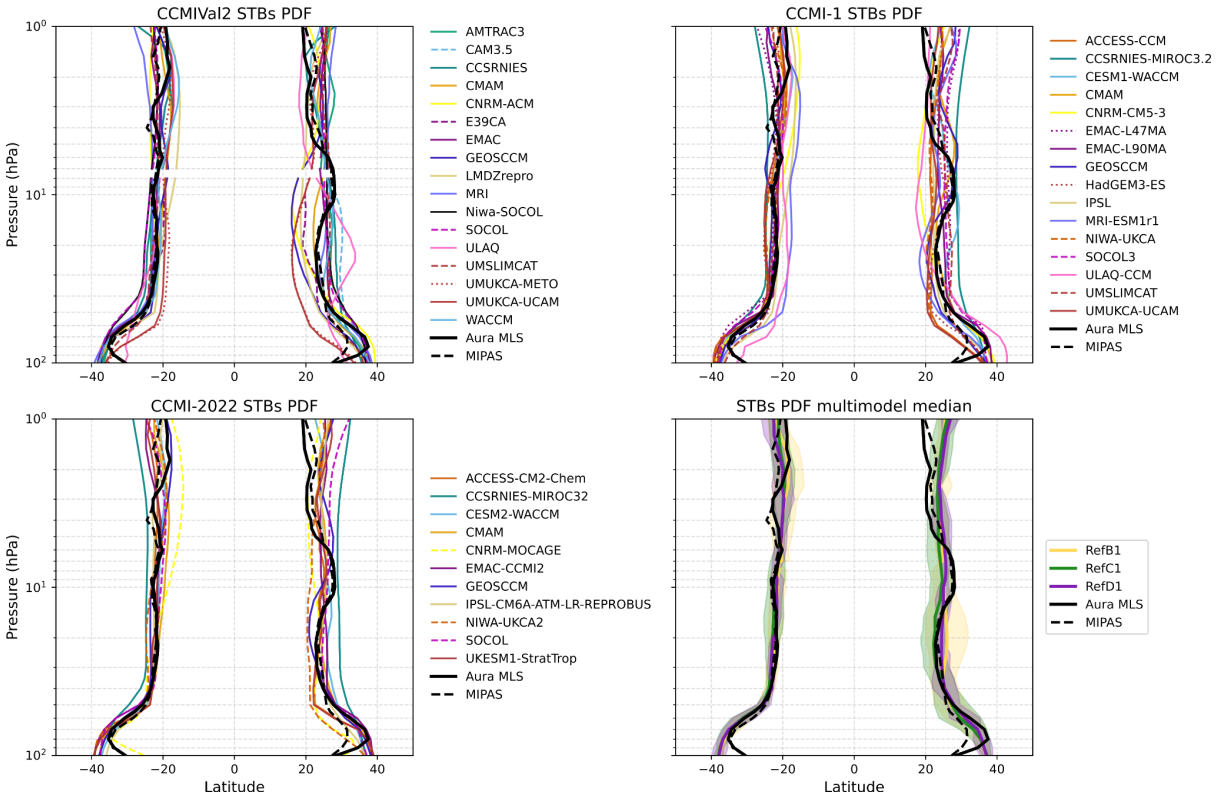

Figure S21. Location of the annual mean subtropical mixing barriers (STBs) computed from the minimum in the N2O PDFs in individual models participating in the three intercomparison initiatives and for the multi-model median of each generation (right bottom panel).

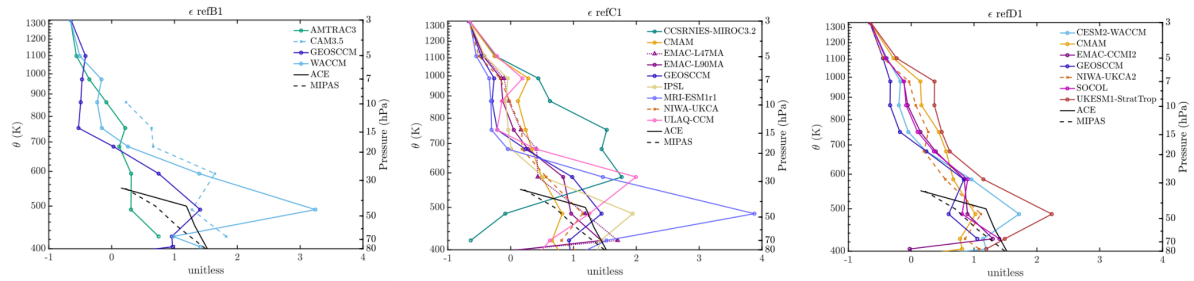

Figure S22. Mixing efficiency calculations from age of air vertical gradient for individual models participating in the three initiatives.

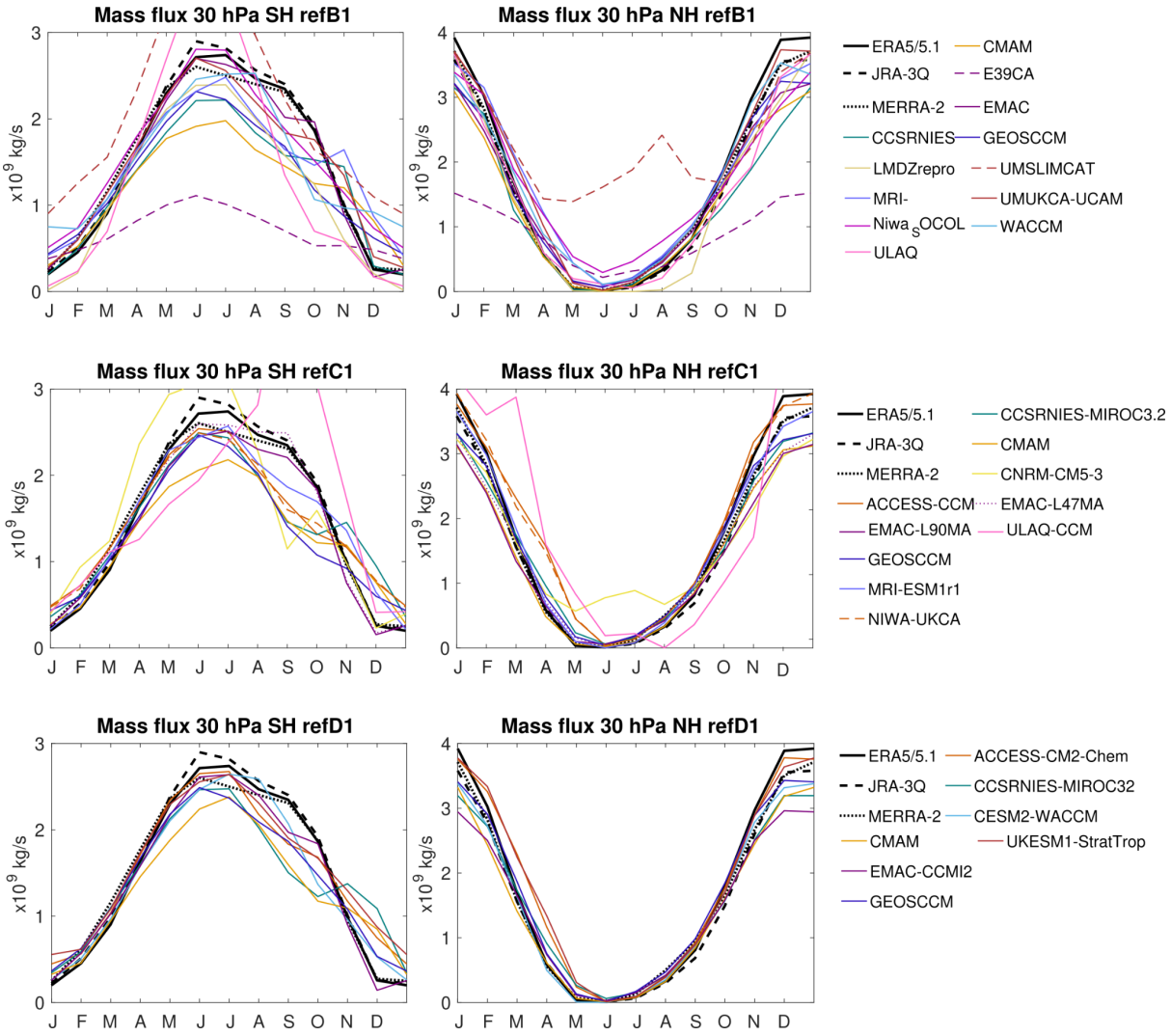

Figure S23. Seasonal cycle of the downward mass flux in the SH (left) and NH (right) in individual models of the three intercomparison initiatives: refB1 (top), refC1 (middle) and refD1 (bottom) simulations.

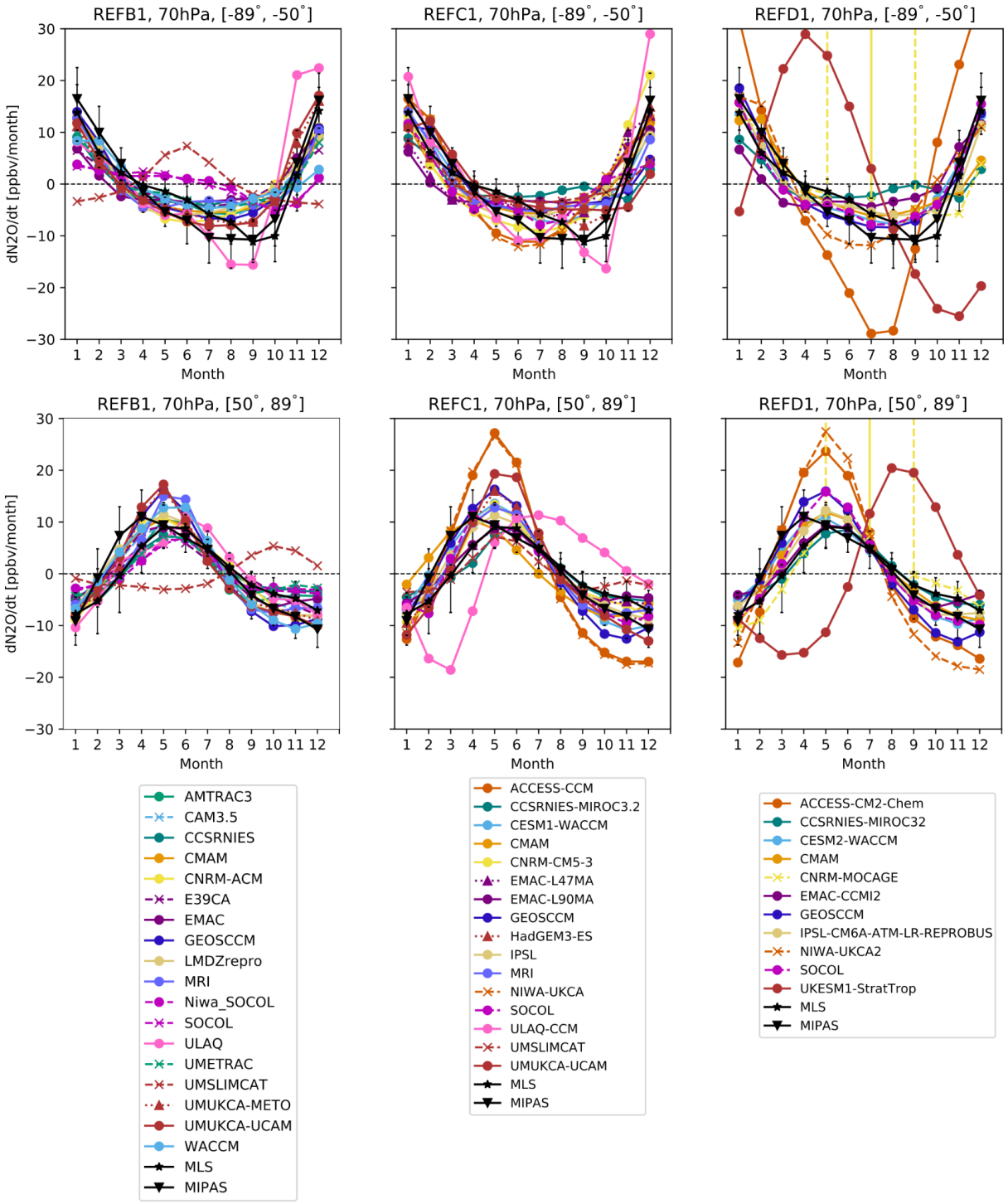

Figure S24. Seasonal cycle of N2O monthly mean tendency in individual models participating in the three intercomparison initiatives and satellite datasets (top: SH, bottom: NH).

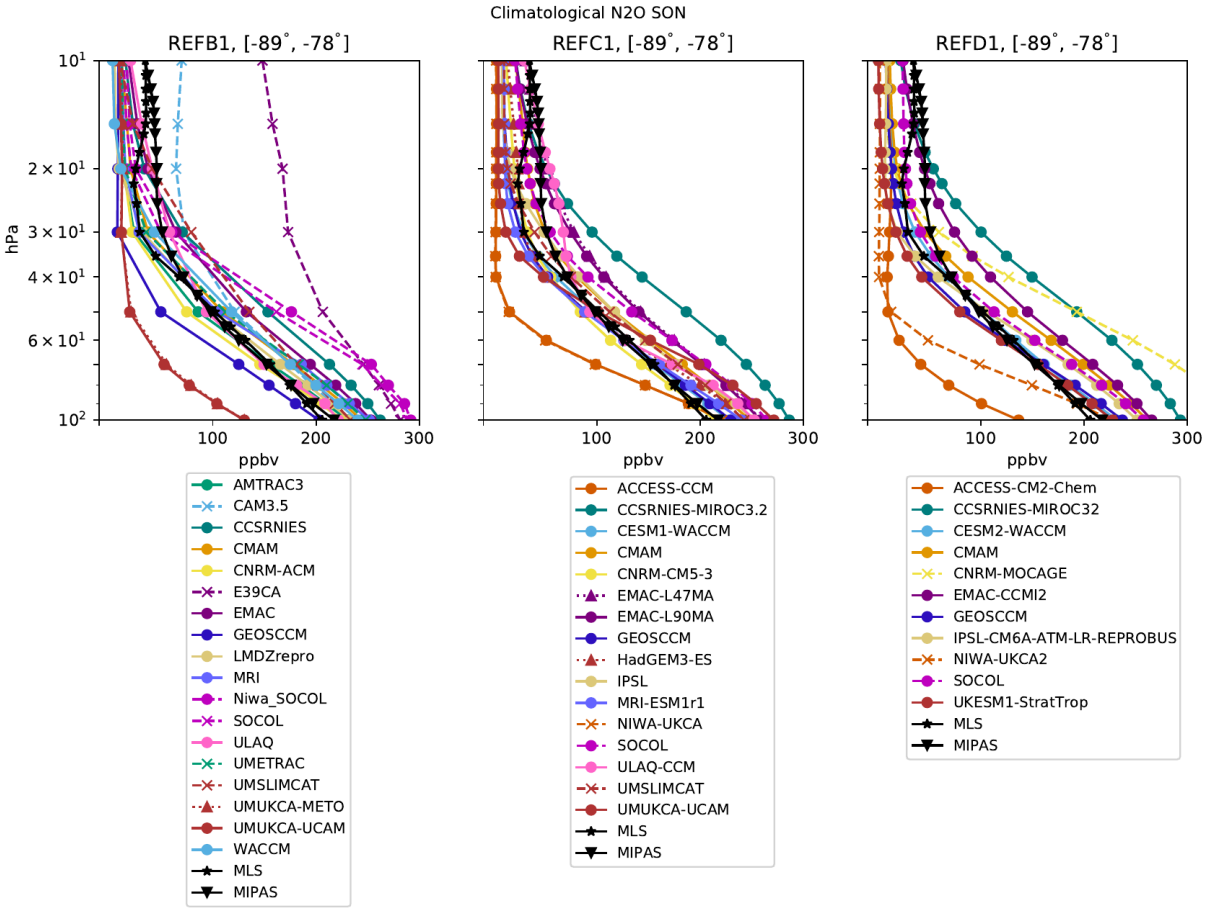

Figure S25. Vertical profile of N2O for individual models participating in the three intercomparison initiatives and satellite datasets.

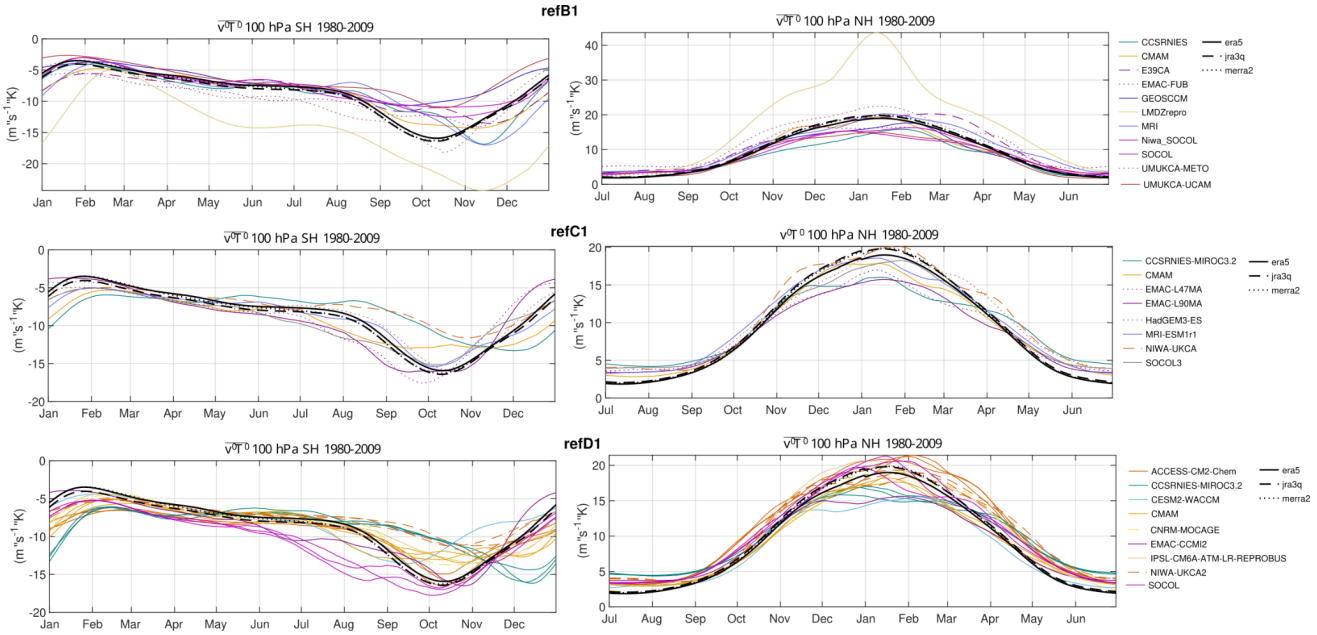

Figure S26. Seasonal cycle of eddy heat flux in the NH (top panels) and SH (bottom panels) for the individual models participating in the three intercomparison initiatives (top.

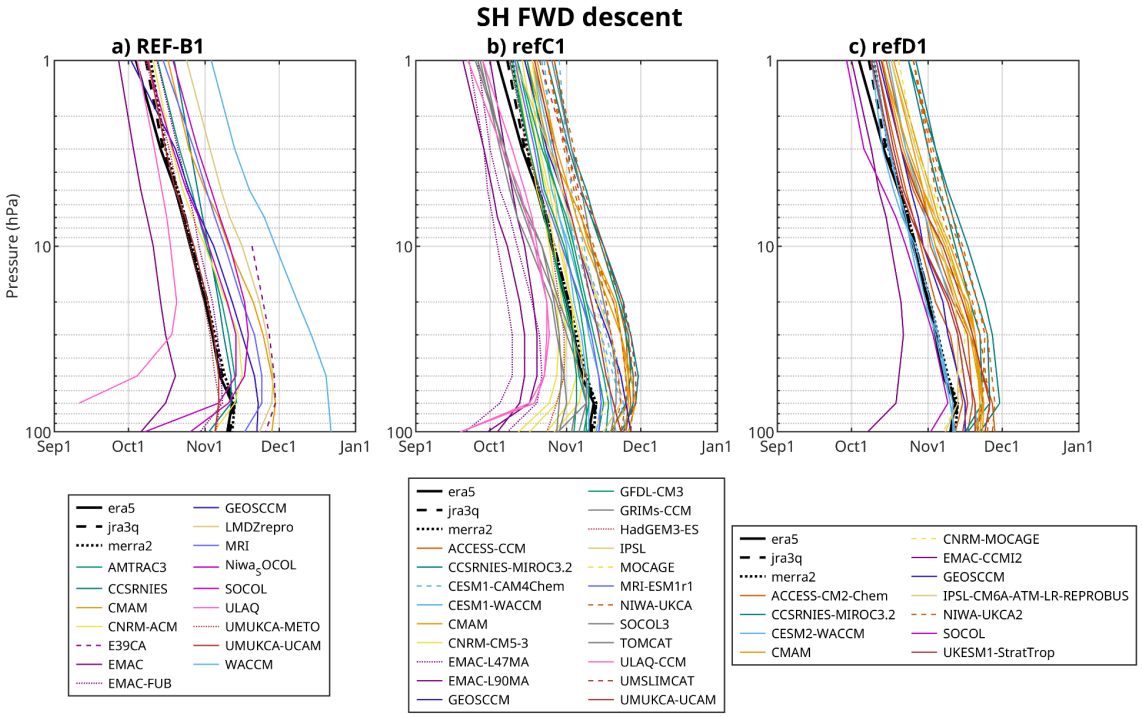

Figure S27. Final warming descent date in the SH for individual models participating in the three intercomparison initiatives.

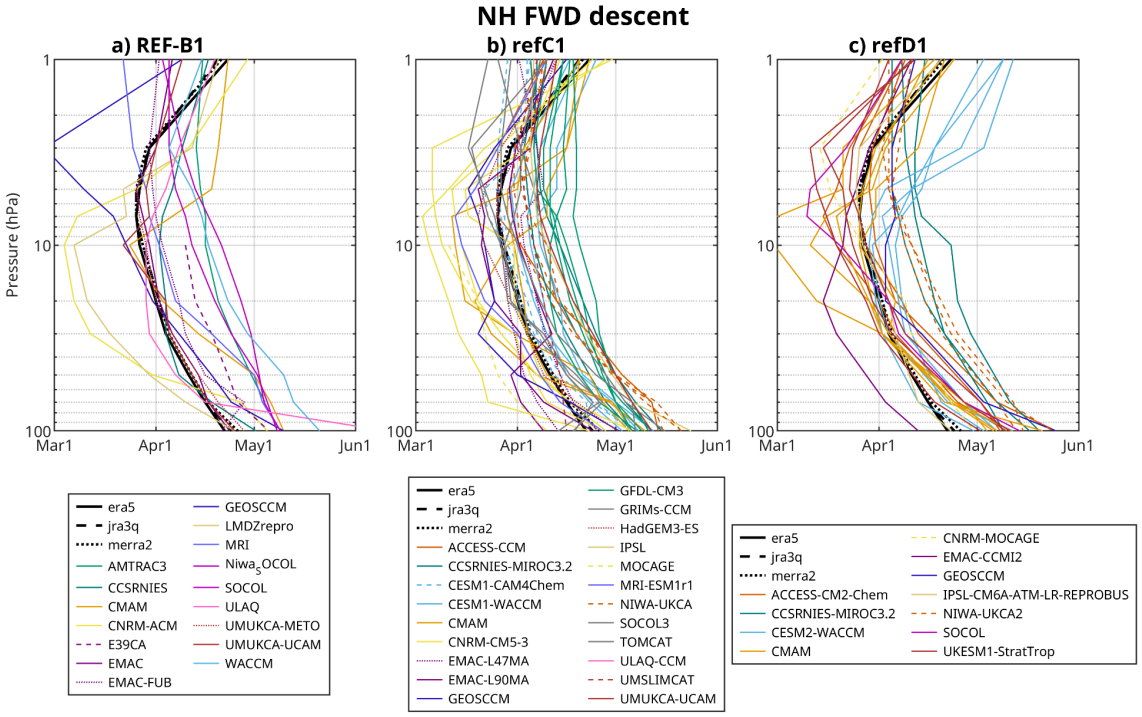

Figure S28. Final warming descent date in the NH for individual models participating in the three intercomparison initiatives.

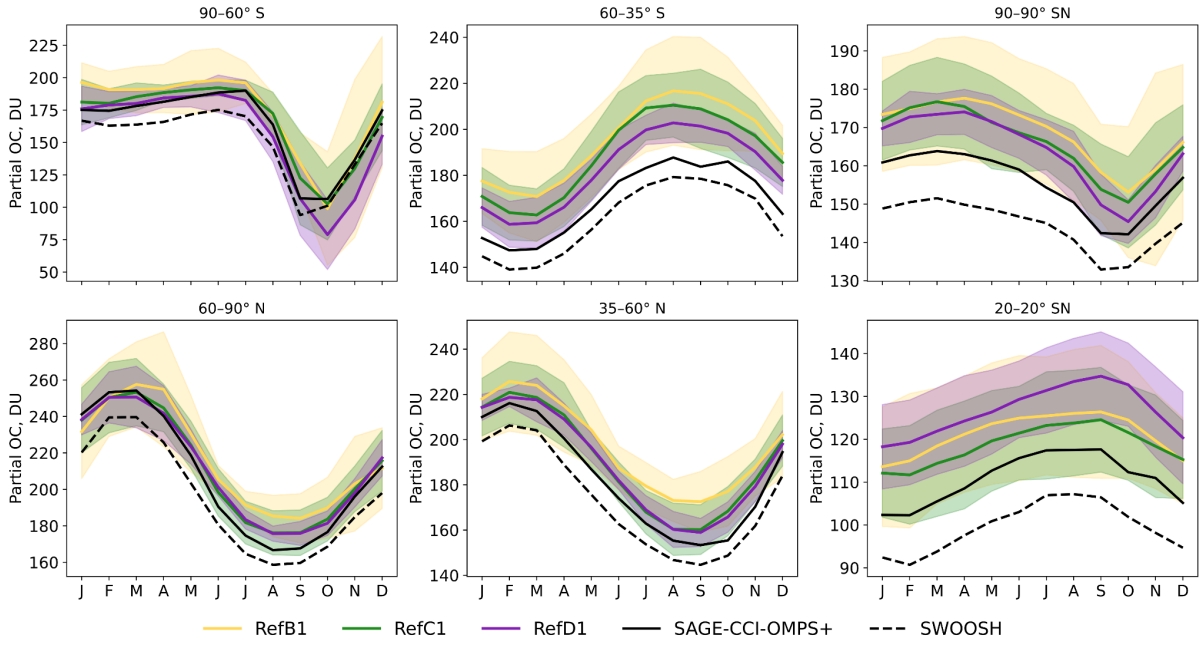

Figure S29. Ozone partial column in the lower stratosphere for different latitude bands and global mean (top right panel). Multi-model mean and MAD computed using all available models (except clear outliers).

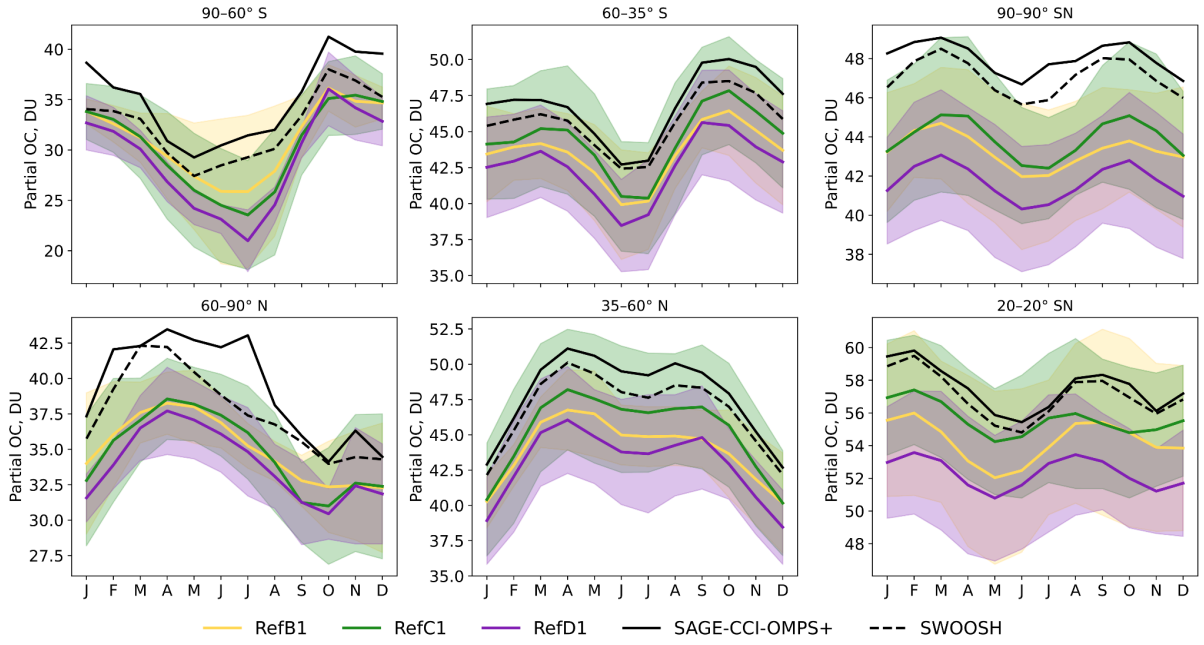

Figure S30. Ozone partial column in the upper stratosphere for different latitude bands and global mean (top right panel). Multi-model mean and MAD computed using all available models (except clear outliers).

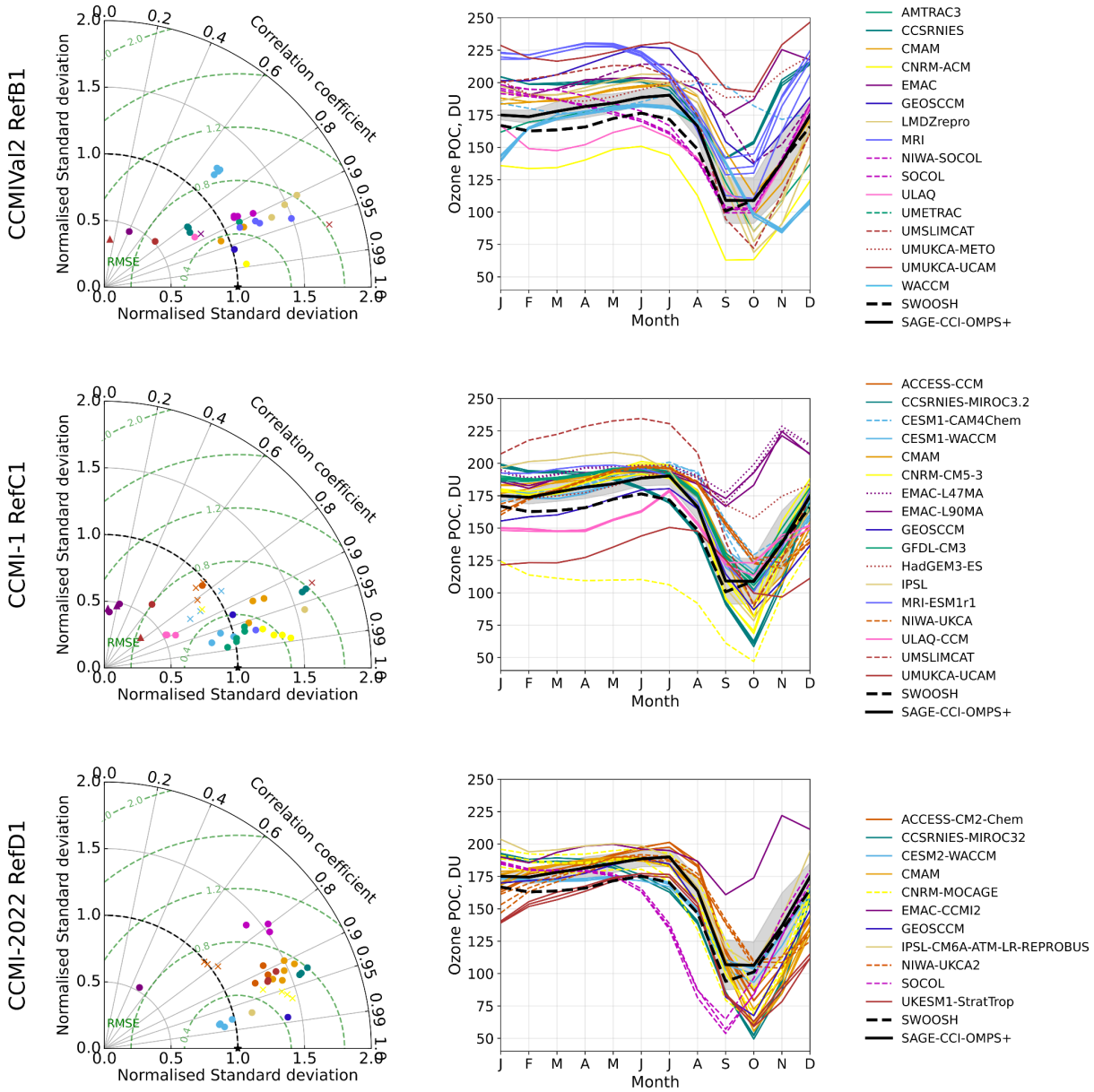

Figure S31. Ozone partial column in the lower stratosphere for the SH polar region (90S-60S) for individual models participating in the three intercomparison initiatives. Left panels: Taylor diagrams. Right panels: seasonal cycle.

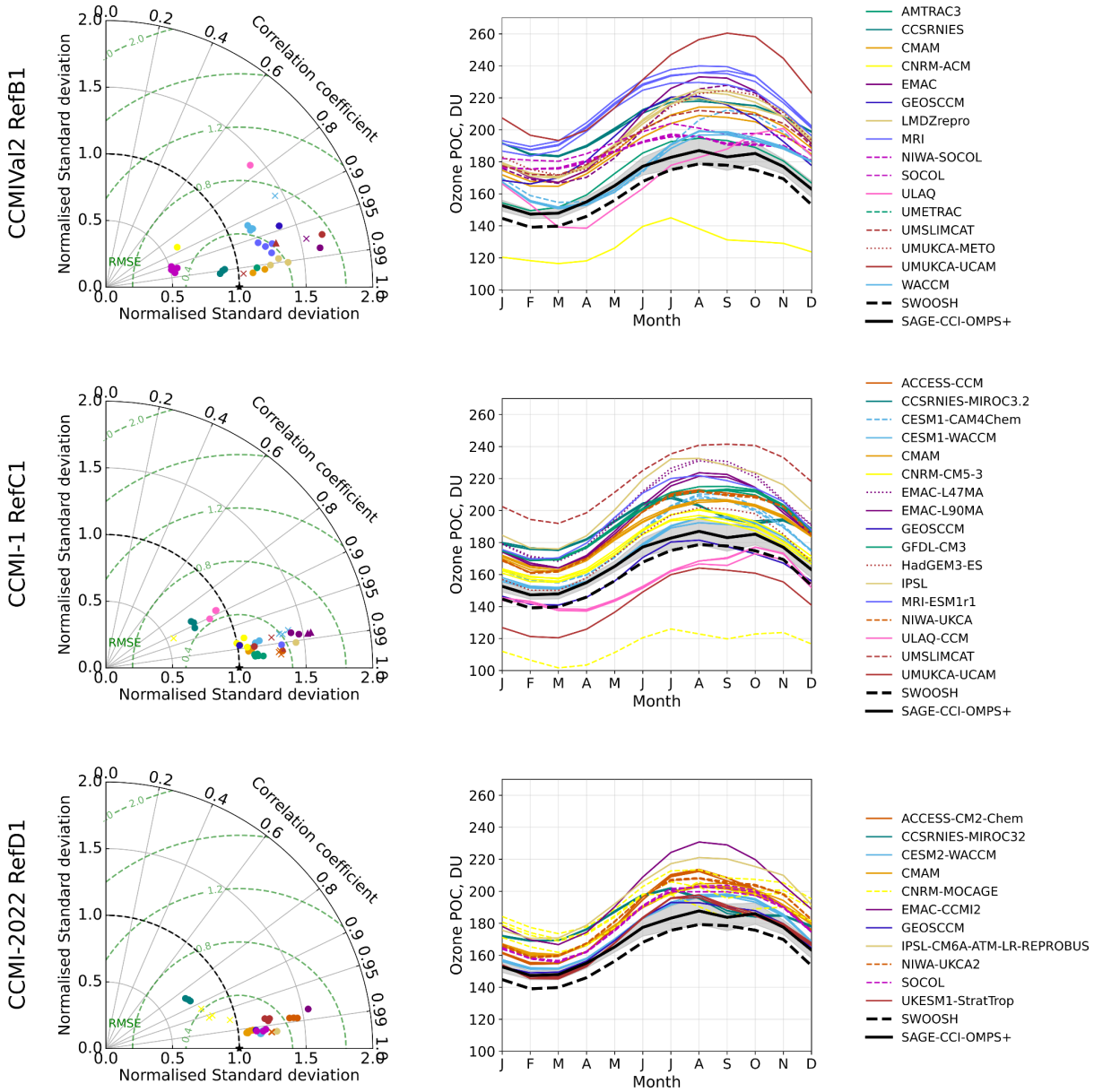

Figure S32. Ozone partial column in the lower stratosphere for the SH midlatitudes region (60S-30S) for individual models participating in the three intercomparison initiatives. Left panels: Taylor diagrams. Right panels: seasonal cycle.

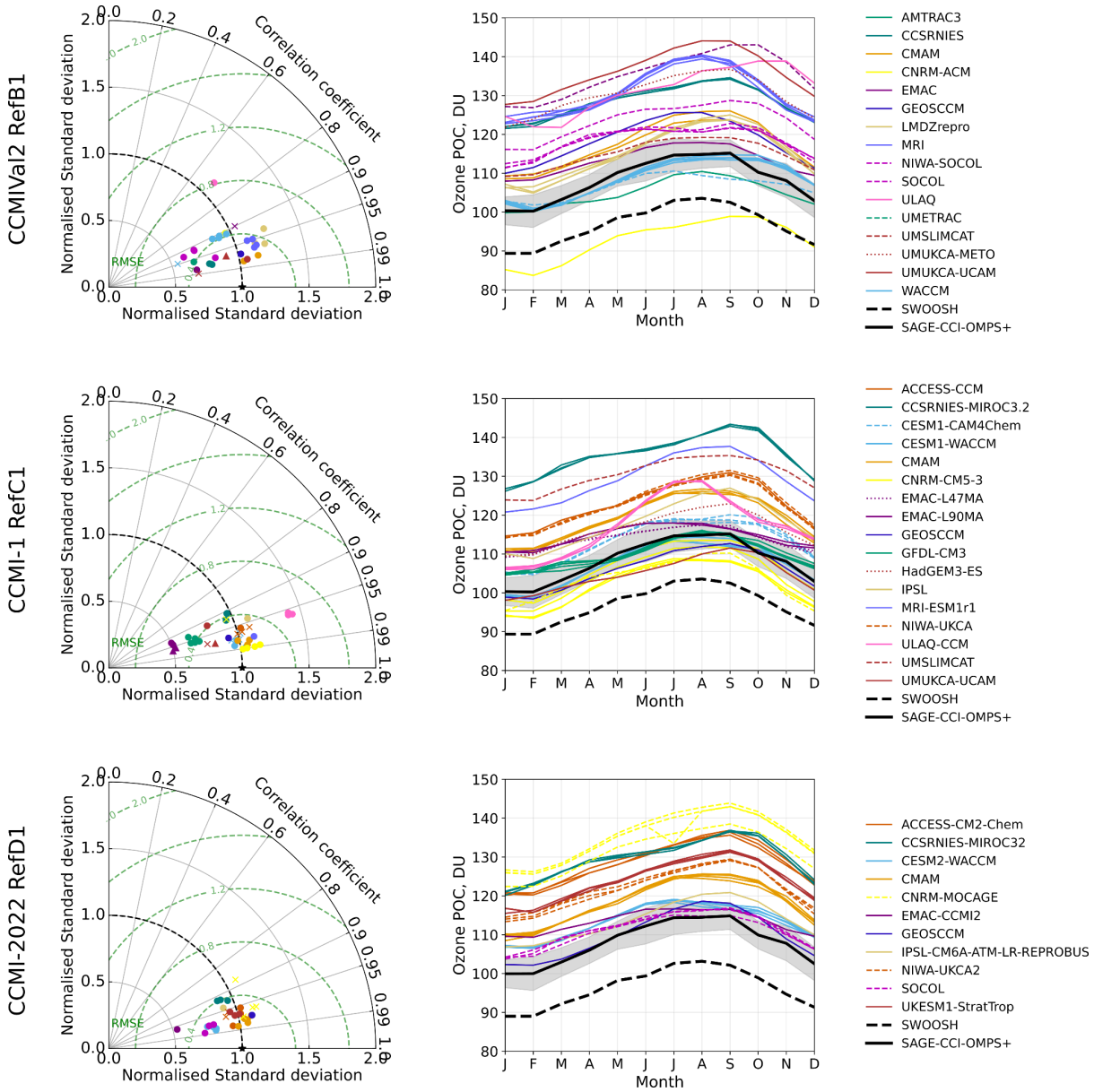

Figure S33. Ozone partial column in the lower stratosphere for the tropics region (20S-20S) for individual models participating in the three intercomparison initiatives. Left panels: Taylor diagrams. Right panels: seasonal cycle.

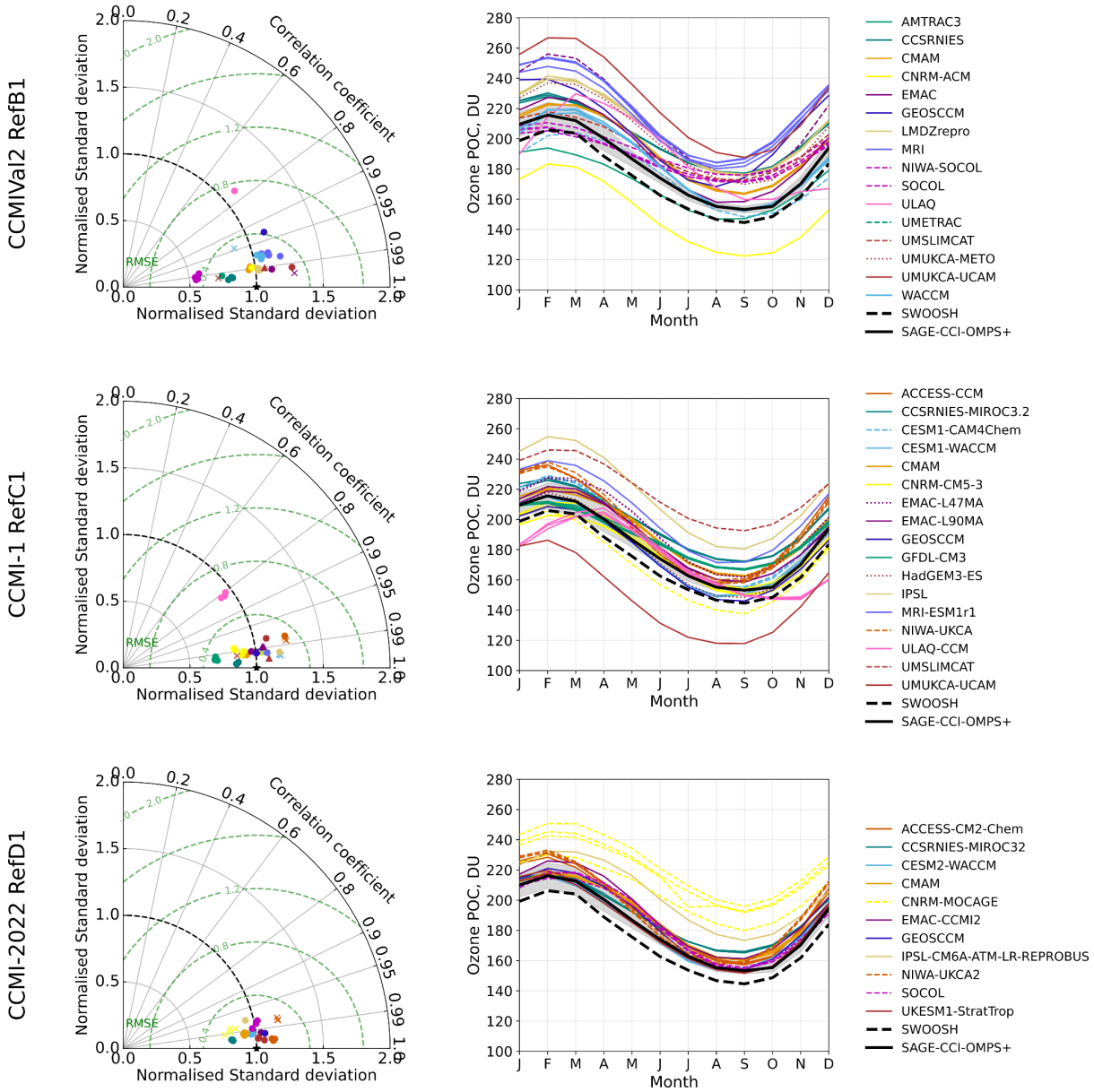

Figure S34. Ozone partial column in the lower stratosphere for the NH midlatitudes region (30N-60N) for individual models participating in the three intercomparison initiatives. Left panels: Taylor diagrams. Right panels: seasonal cycle.

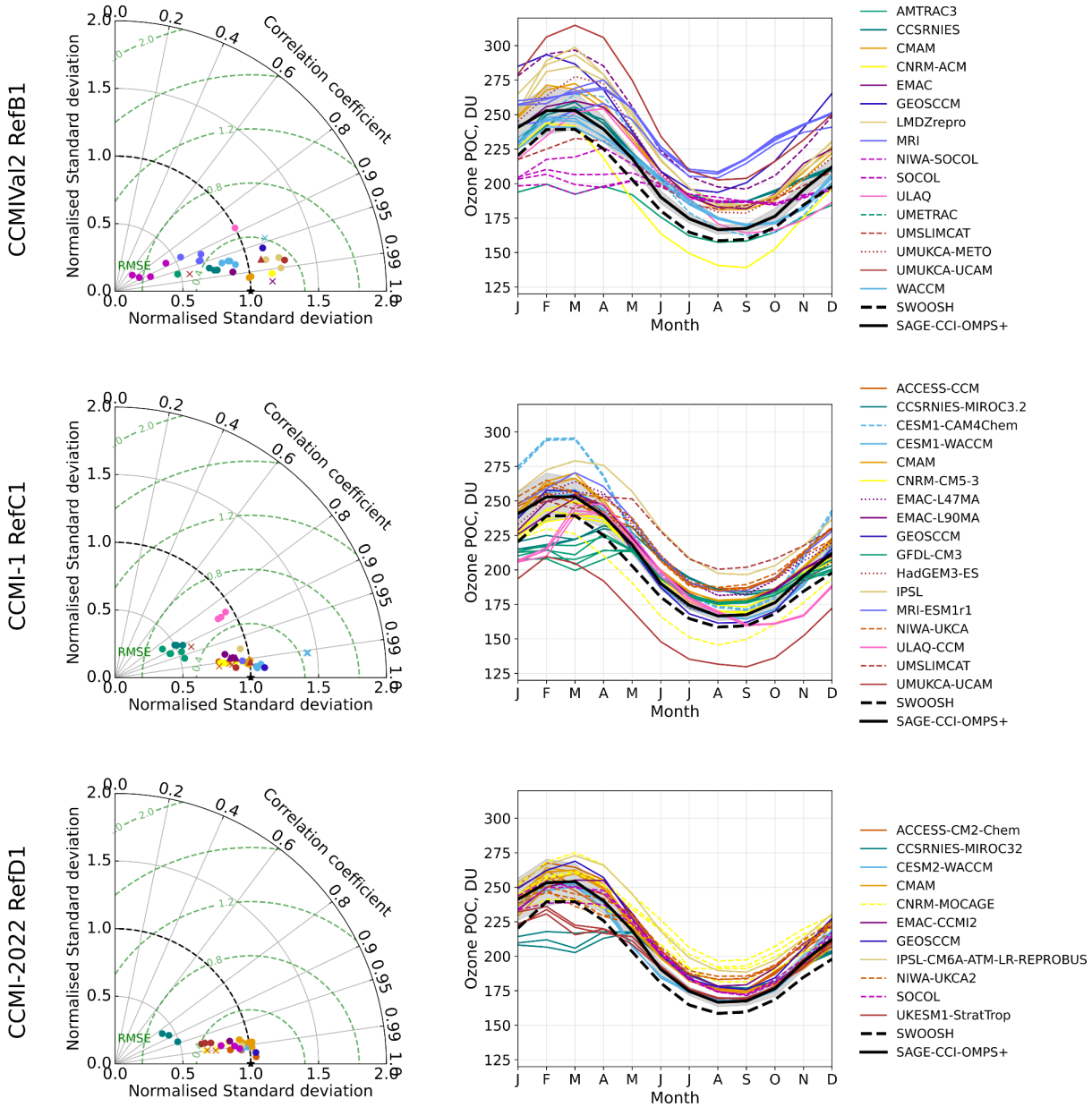

Figure S35. Ozone partial column in the lower stratosphere for the NH polar region (60N-90N) for individual models participating in the three intercomparison initiatives. Left panels: Taylor diagrams. Right panels: seasonal cycle.

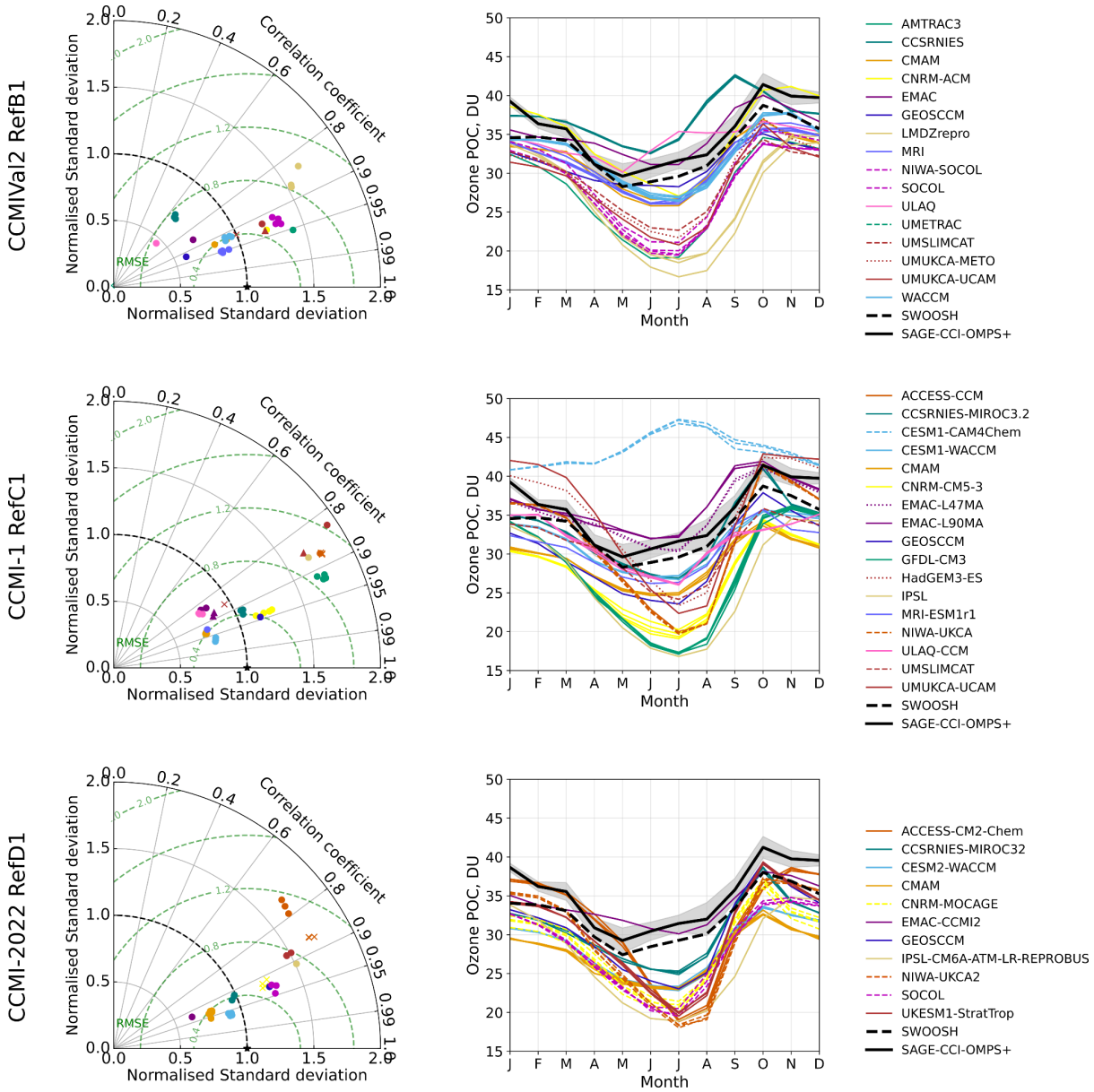

Figure S36. Ozone partial column in the upper stratosphere for the SH polar region (90S-60S) for individual models participating in the three intercomparison initiatives. Left panels: Taylor diagrams. Right panels: seasonal cycle.

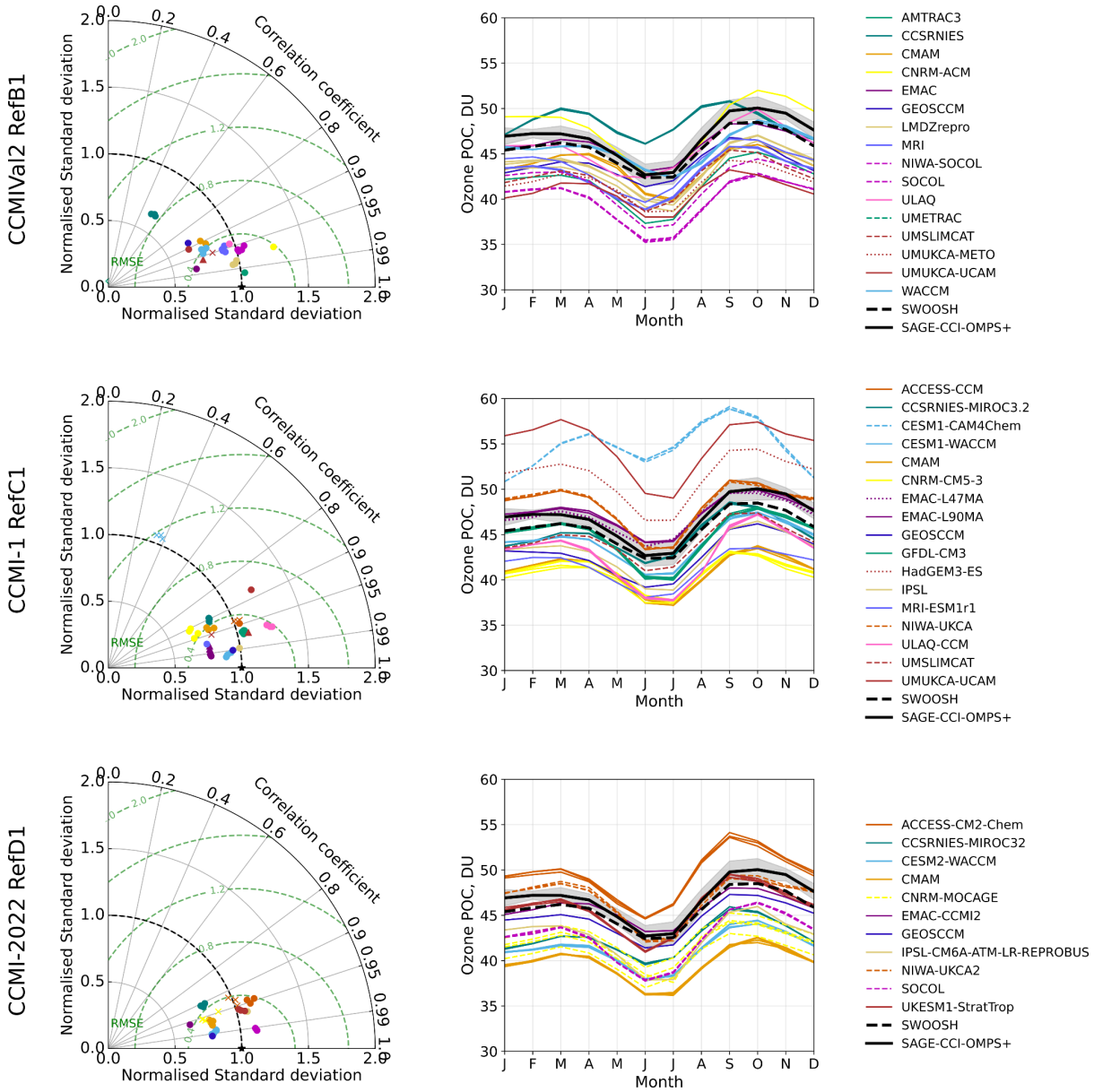

Figure S37. Ozone partial column in the upper stratosphere for the SH midlatitudes region (60S-30S) for individual models participating in the three intercomparison initiatives. Left panels: Taylor diagrams. Right panels: seasonal cycle.

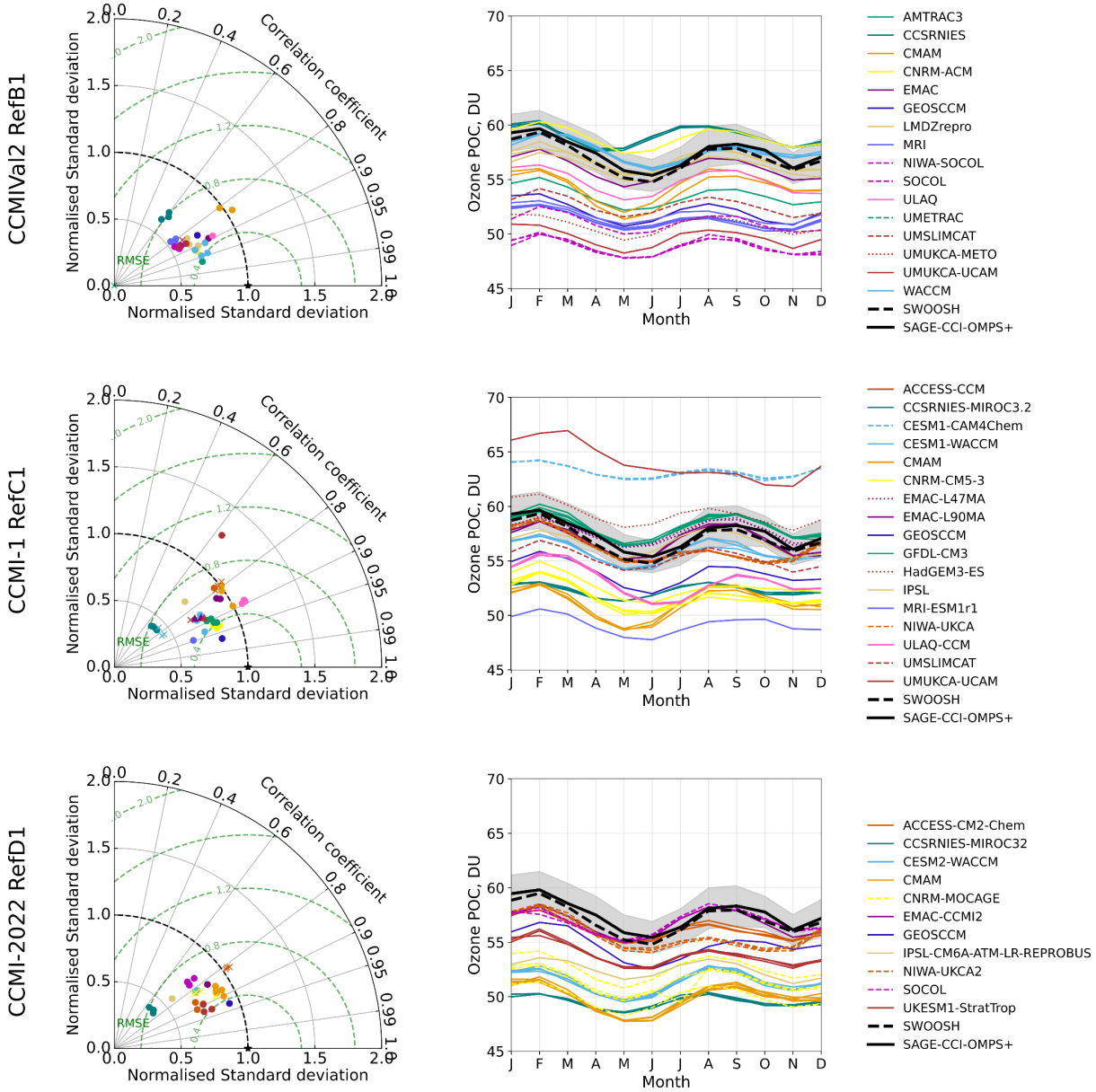

Figure S38. Ozone partial column in the upper stratosphere for the tropics region (20S-20S) for individual models participating in the three intercomparison initiatives. Left panels: Taylor diagrams. Right panels: seasonal cycle.

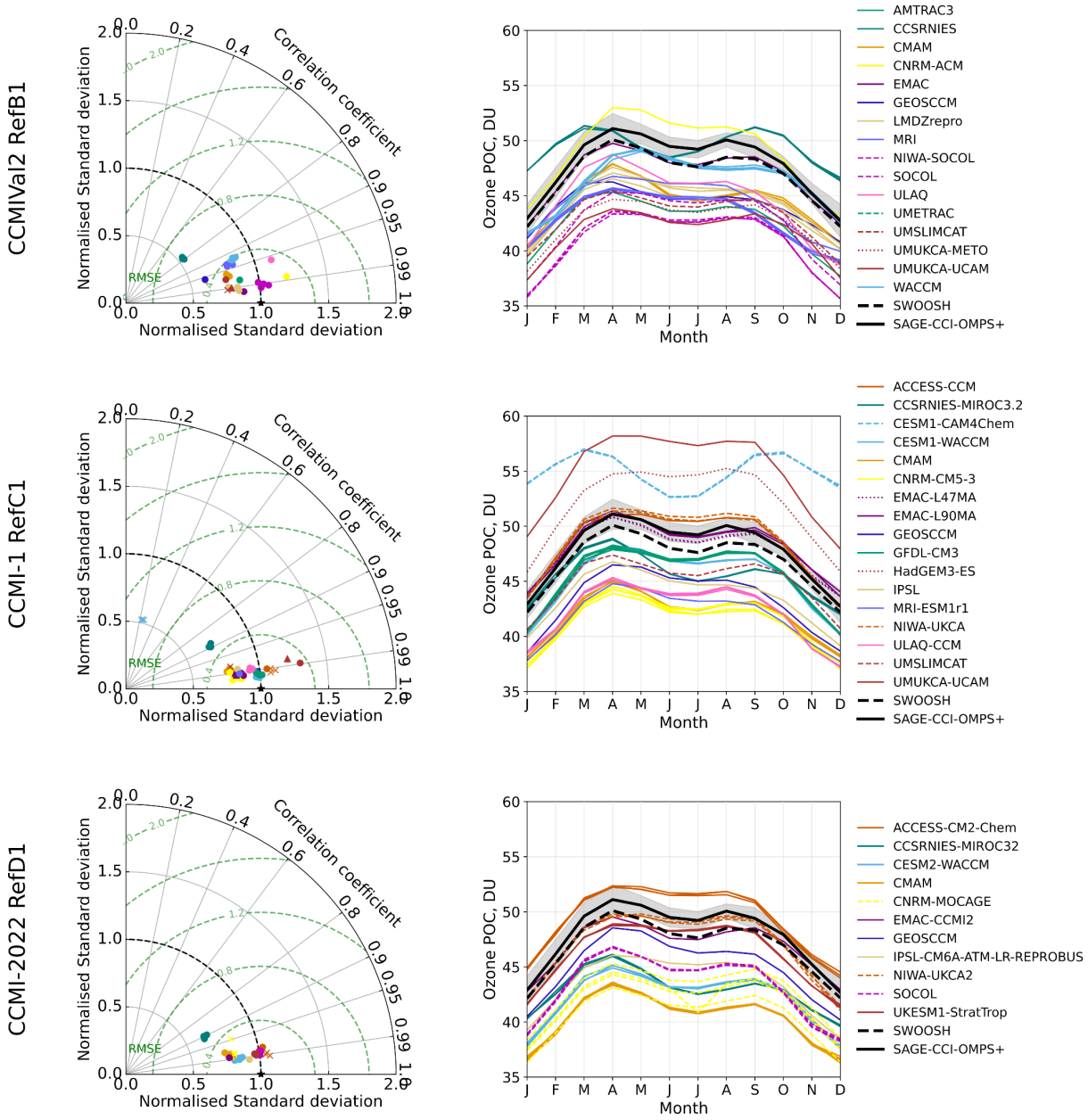

Figure S39. Ozone partial column in the upper stratosphere for the NH midlatitudes region (30N-60N) for individual models participating in the three intercomparison initiatives. Left panels: Taylor diagrams. Right panels: seasonal cycle.

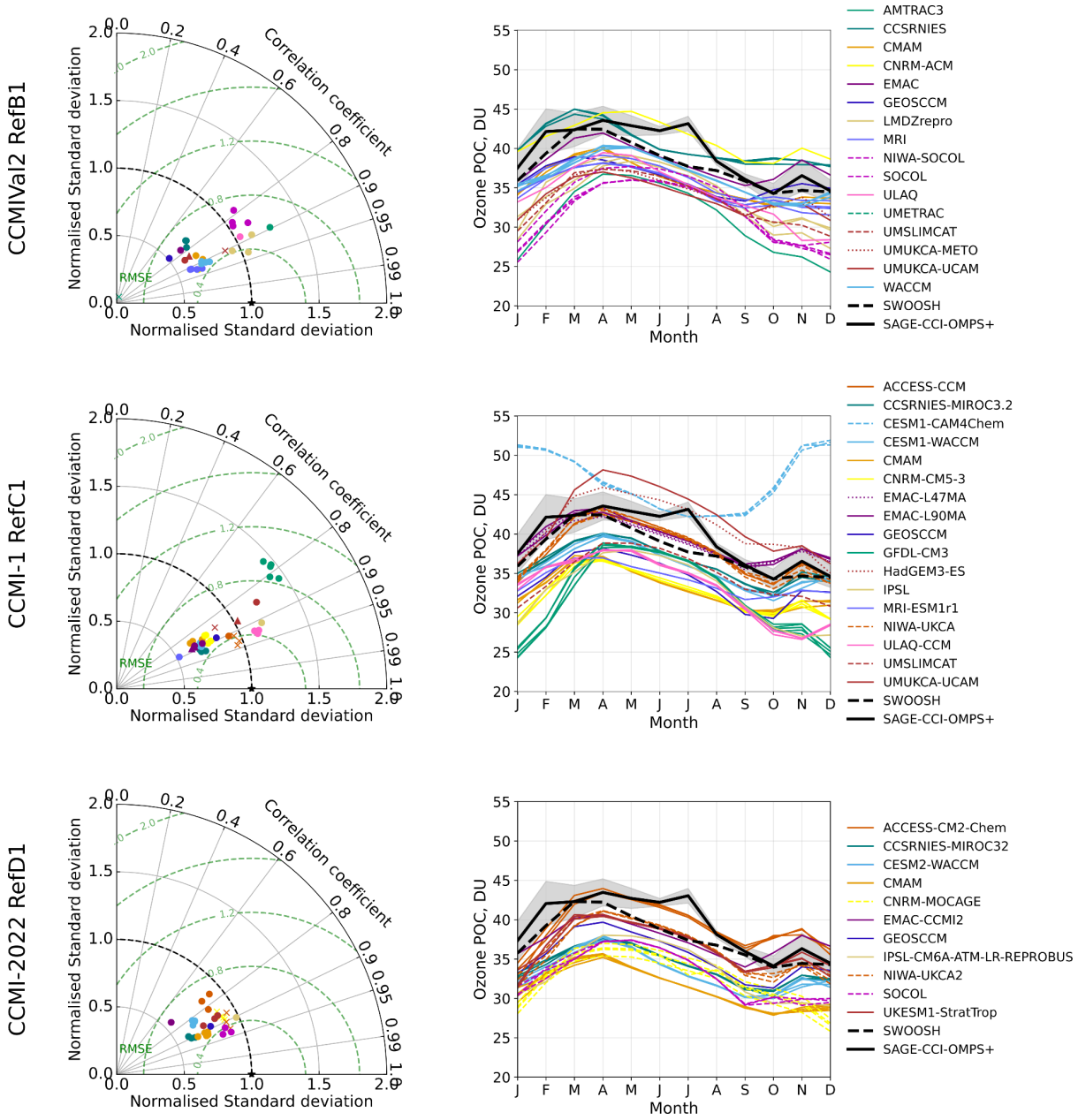

Figure S40. Ozone partial column in the upper stratosphere for the NH polar region (60N-90N) for individual models participating in the three intercomparison initiatives. Left panels: Taylor diagrams. Right panels: seasonal cycle.

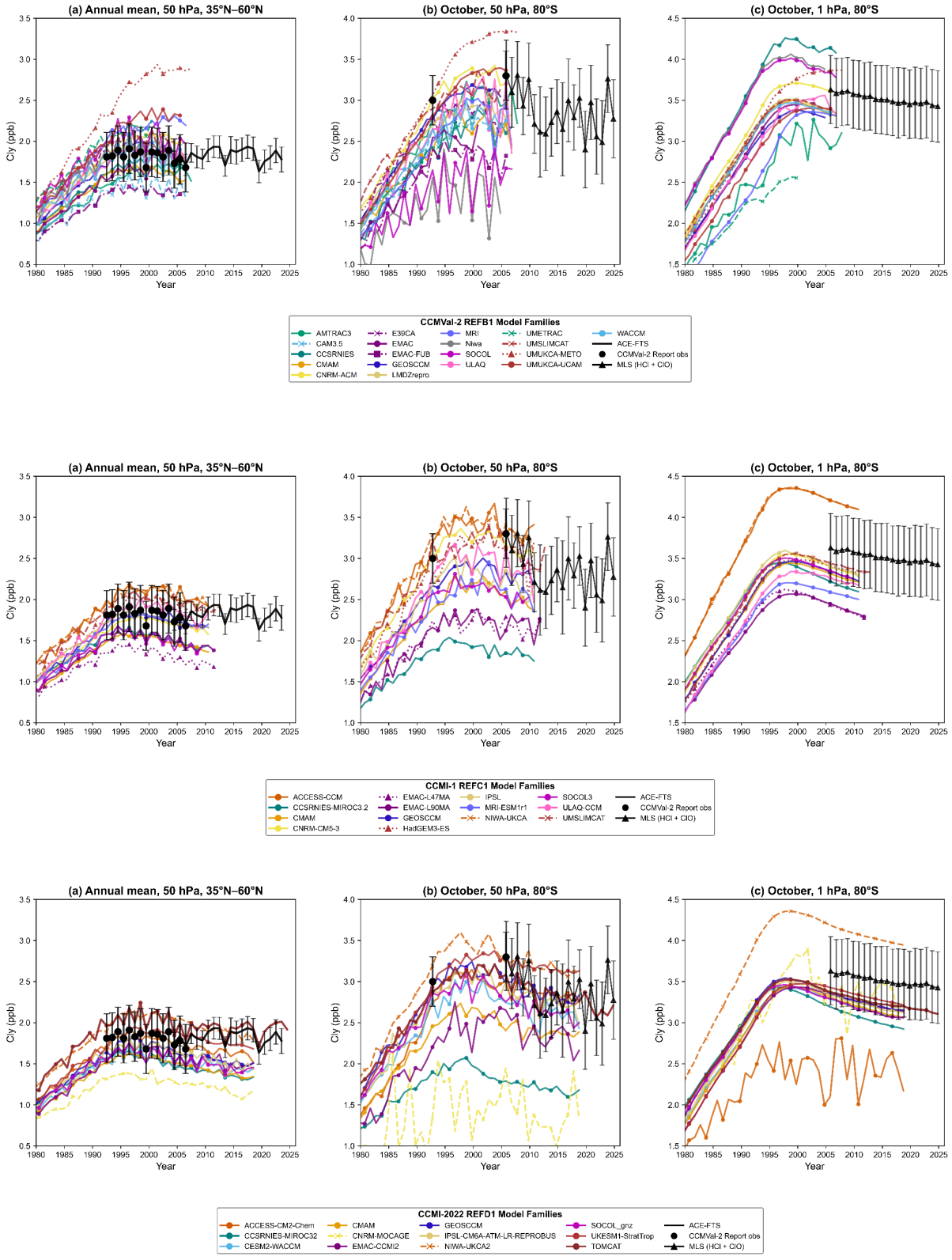

Figure S41. Timeseries of Cly in individual models participating in the three intercomparison initiatives. All models are shown, while in the main manuscript median plots the following models are removed: CCMVal-2 refB1: UMUKCA-METO, AMTRAC3, UMETRAC; CCMI-1 refC1: NIWA-UKCA, ACCESS-CCM; CCMI-2022 refD1: CNRM-MOCAGE, ACCESS-CM2-Chem, NIWA-UKCA2.

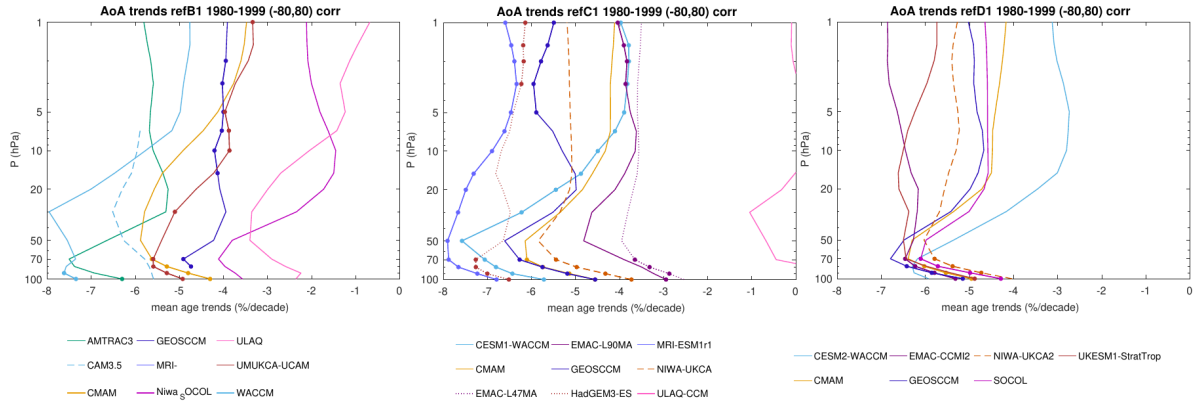

Figure S42. Trends in mean age of air in individual models participating in the three intercomparison initiatives.

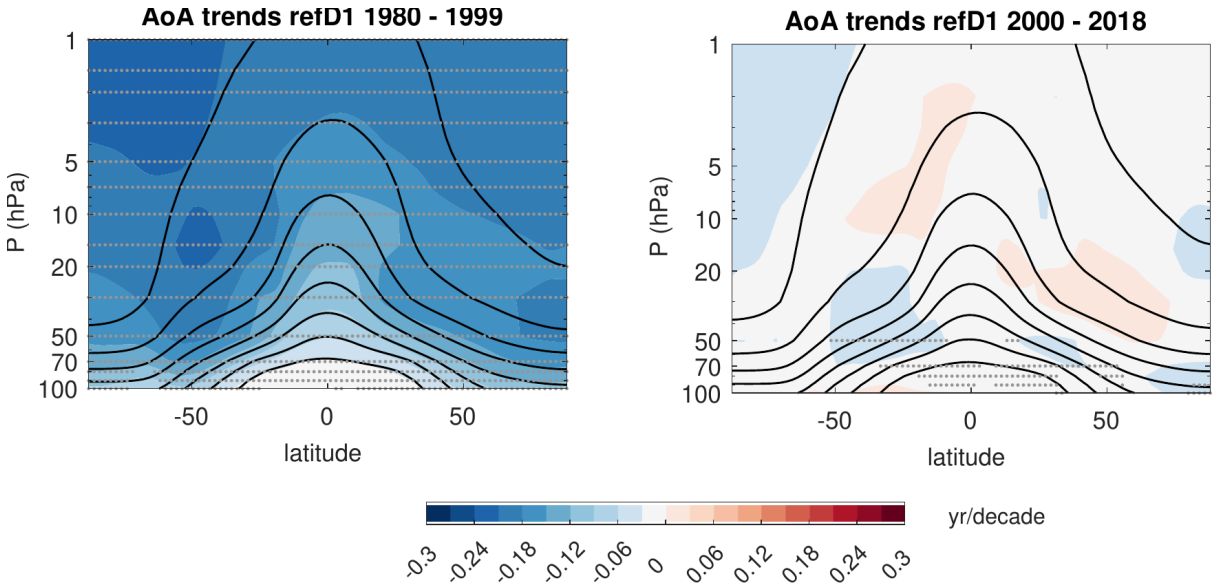

Figure S43. Trends in mean age of air for pre- and post-2000 periods for the multimodel mean. In contrast to Fig. 18 in the main document, here no variability is removed before computing the linear trends.

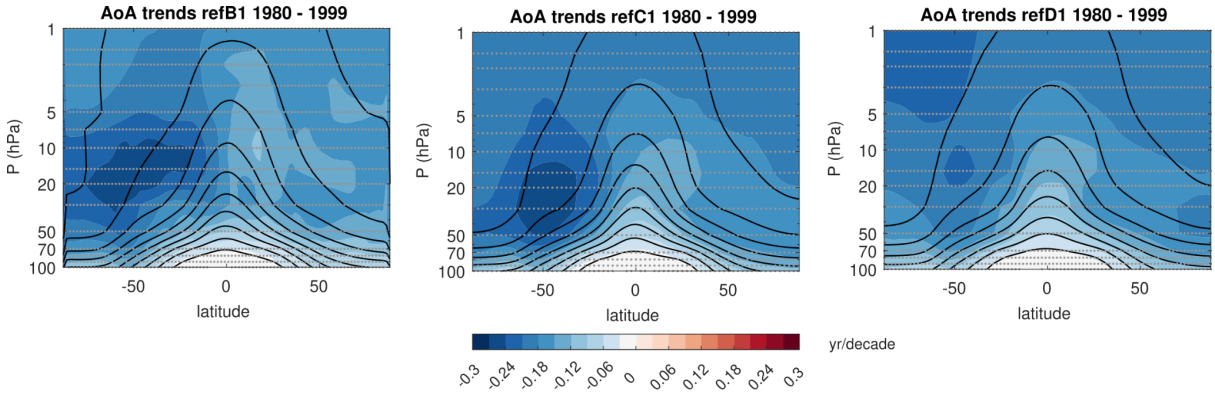

Figure S44. Trends in mean age of air over 1980-1999 for the multimodel mean of CCMVal-2 (left), CCMI-1 (center) and CCMI-2022 (right). In contrast to Fig. 18 in the main document, here no variability is removed before computing the linear trends.

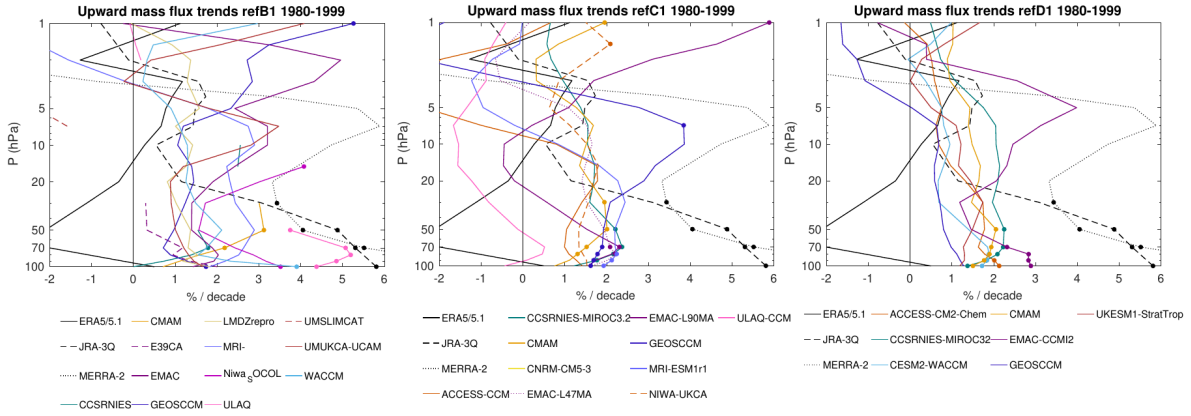

Figure S45. Trends in upward mass flux in individual models participating in the three intercomparison initiatives.

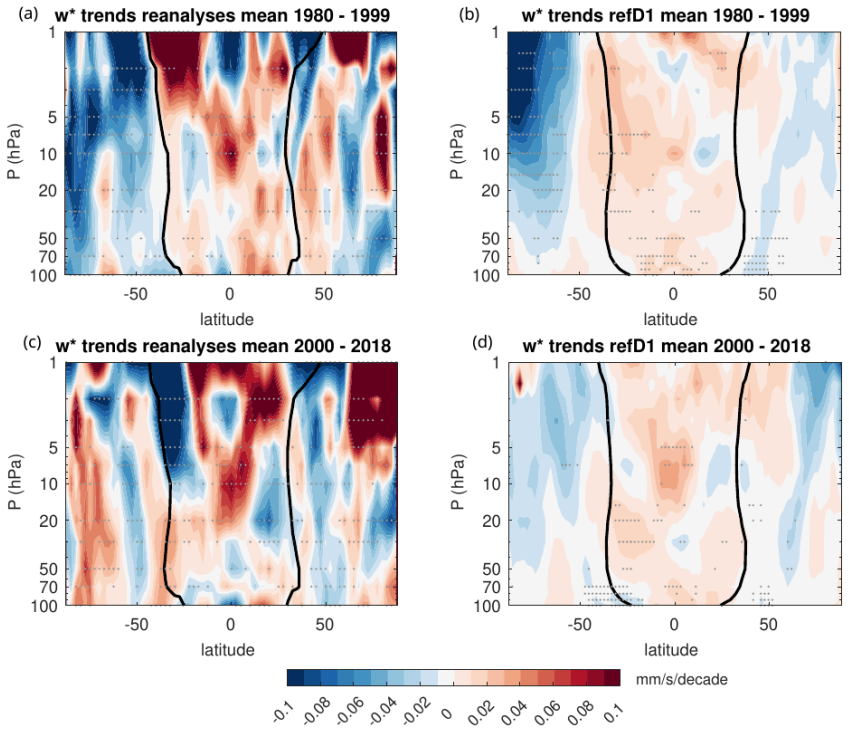

Figure S46. Trends in the vertical component of the residual circulation for pre- and post-2000 periods for the multimodel mean (b and d) and for the multi-reanalysis mean (a and c). In contrast to Fig. 19 in the main document, here no variability is removed before computing the linear trends trends.

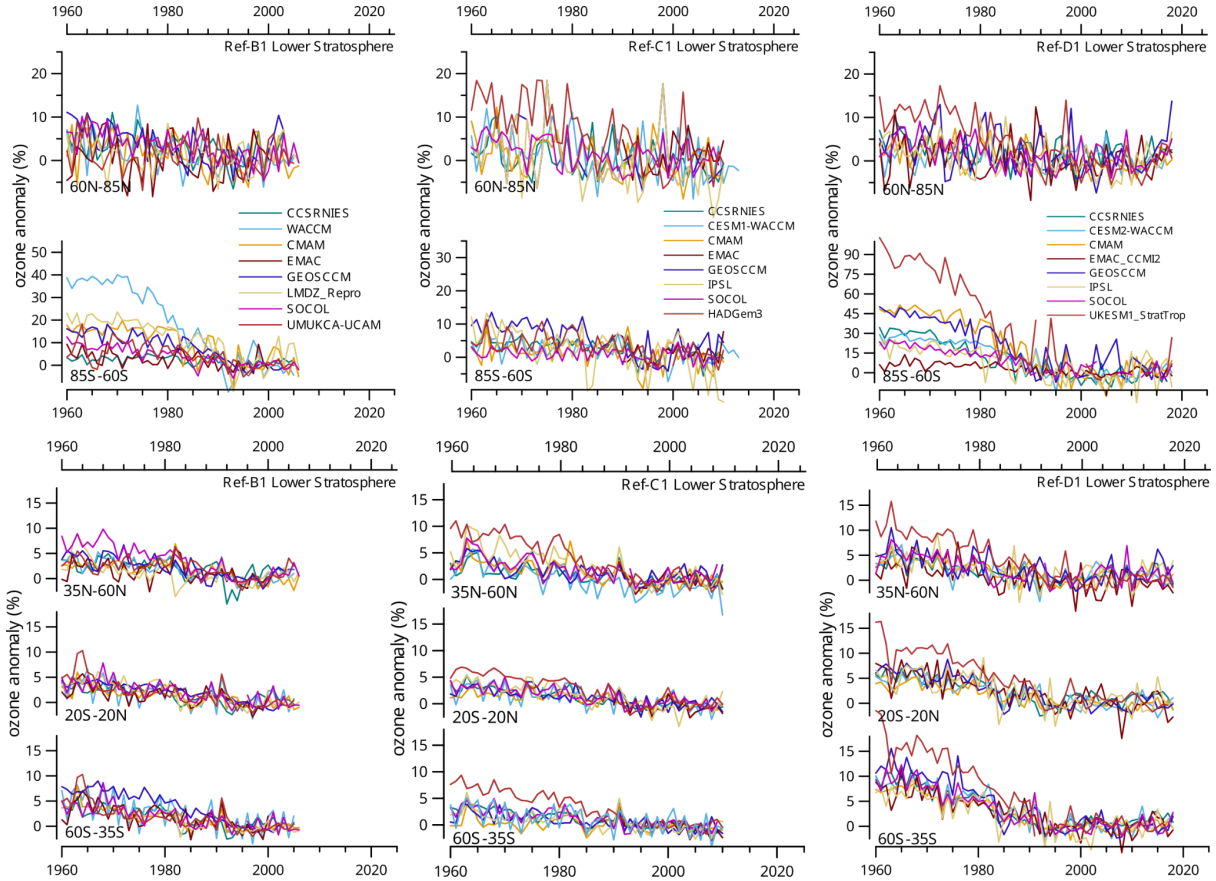

Figure S47. Timeseries of ozone partial column anomalies for the lower stratosphere in individual models participating in the three intercomparison initiatives.

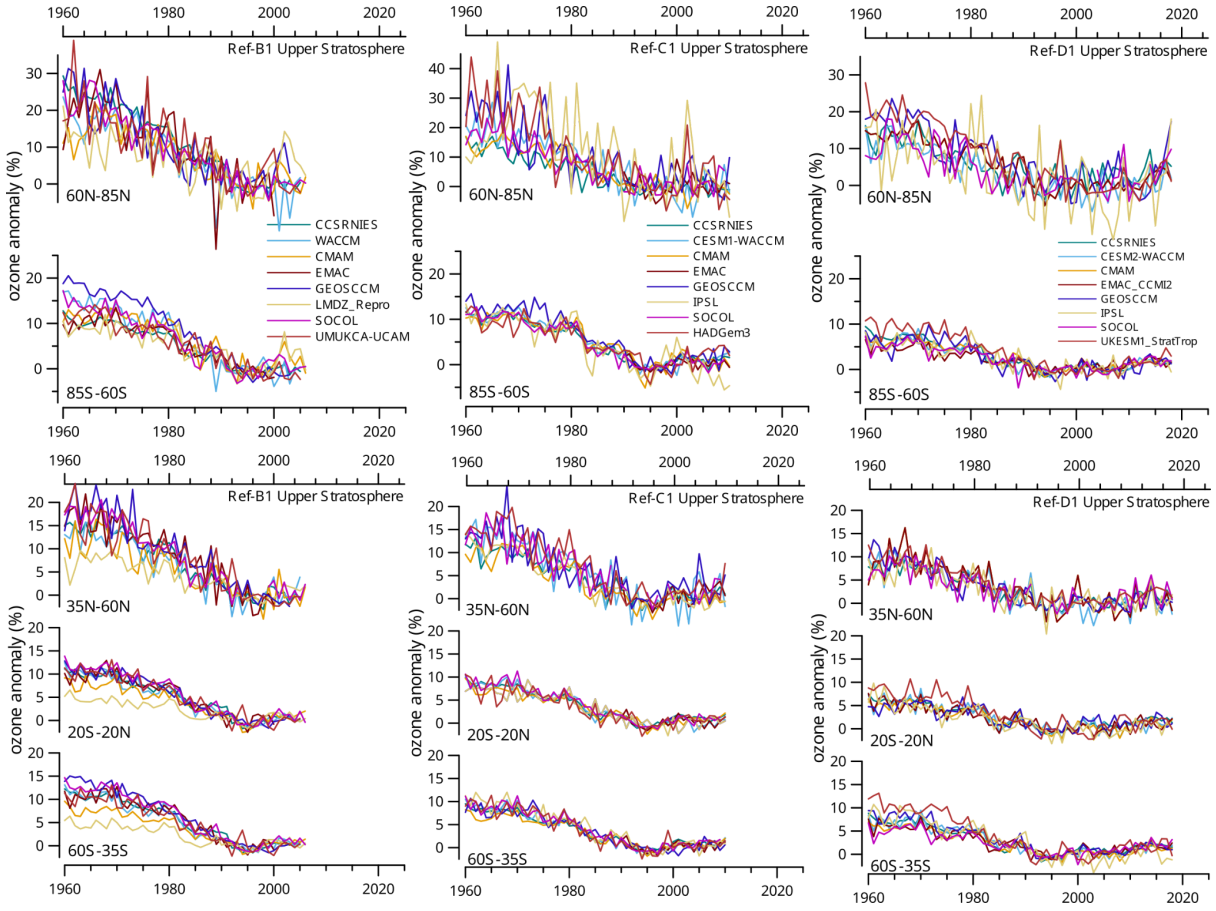

Figure S48. Timeseries of ozone partial column anomalies for the upper stratosphere in individual models participating in the three intercomparison initiatives.